Broadband Modelling of High-Frequency Devices and Circuits

by

Douglas Paul

A thesis submitted to the Faculty of Graduate Studies and Research in partial fulfillment of the requirements for the degree of Master of Applied Sciences

Ottawa-Carleton Institute for Electrical and Computer Engineering

Department of Electronics

Faculty of Engineering

Carleton University

Ottawa, Ontario, Canada

September 2006

Your file Votre référence
ISBN: 978-0-494-18330-4
Our file Notre référence
ISBN: 978-0-494-18330-4

Abstract

Equivalent-circuit models are a popular way to model circuit devices among designers. As the operating frequencies of circuits continue to increase, these models must be improved to account for additional effects seen under these conditions. Traditional efforts to improve equivalent circuit models are device-specific, laborious and ad-hoc in nature.

To address these difficulties, this thesis presents an efficient and automated algorithm which identifies augmenting equivalent circuits to improve the accuracy of simple equivalent-circuit models over a frequency range of interest. This algorithm is generic in the sense that it can be applied to any multi-port equivalent-circuit model for a device whose performance can be described by y-parameters. Therefore, it has a wide range of applications. As the algorithm uses single-port networks as augmentations, existing passivity enforcement techniques are simplified, ensuring realizable augmentations.

Acknowledgements

I would like to express my appreciation to my supervisors, Professors Michel Nakhla and Ram Achar. They provided the initial inspiration for this work and gave critical guidance throughout the process. I would also like to thank Professor Andreas Weisshaar of Oregon State University for his helpful comments and insight during the development of the algorithm and the study of its application.

Contents

List of Figures

List of Tables

List of Symbols

$\mathbf{0}_{m\times n}$ Zero matrix of dimension $m \times n$.

$\boldsymbol{\xi}$ Selector vector giving node connection information of a model augmentation

ϕ Value of a circuit component undergoing sensitivity analysis

ω Frequency

$\boldsymbol{A}$ The MNA matrix

$\boldsymbol{B}$ Selector matrix specifying port voltage source connections to the MNA system

$\boldsymbol{b}$ Right-hand-side vector of the linear system formulation $\boldsymbol{Ax} = \boldsymbol{b}$

$\boldsymbol{C}$ Frequency-dependent part of the MNA matrix

$\boldsymbol{G}$ Frequency-independent part of the MNA matrix

$\boldsymbol{i}$ Vector of port currents

s Independent variable of the Laplace domain (compare with t in the time domain)

$\boldsymbol{v}$ Vector of port excitation voltage source magnitudes

$\boldsymbol{x}$ Vector of MNA system variables

$\boldsymbol{Y}$ y-parameters of an S-ECM

$\boldsymbol{Y}_{\text{meas}}$ y-parameters of a measured device

$\Delta\boldsymbol{Y}$ Difference between modelled and measured y-parameters of a multi-port network

$\hat{\boldsymbol{Y}}$ y-parameters of an A-ECM

$z_{\text{aug,par}}$ Driving-point impedance of a single-port augmentation connected in parallel with an existing model component

$z_{\text{aug,ser}}$ Driving-point impedance of a single-port augmentation connected in series with an existing model component

Abbreviations

A-ECM Augmented Equivalent-Circuit Model – an S-ECM that has had augmenting networks added to it using the algorithm proposed in this thesis

DC Direct Current – circuit operation at a frequency of 0 Hz

ECM Equivalent-Circuit Model – a model of a device composed of standard circuit elements

EM Electromagnetic

FET Field-Effect Transistor

KCL Kirchhoff's Current Law

MNA Modified Nodal Analysis – a technique for analysing circuits

RLCG Resistance-Inductance-Capacitance-Conductance – in reference to the characteristics of a transmission line

S-ECM Simple Equivalent-Circuit Model – an ECM developed using traditional techniques, usually low order and valid over a limited frequency range

Chapter 1

Introduction

1.1 Background and Motivation

As the operating frequencies of designs continue to rise, there is an increasing demand for device models that are valid over broader ranges of frequencies. Typical designs today require device characterization spanning in the range of 1-10 GHz and it continues to rise rapidly. From a designer's perspective, the use of equivalent-circuit models to characterize the multi-port parameters, either measured or simulated, of the device is attractive. These equivalent circuits use basic circuit elements to model the response of a complex device and are very intuitive from the perspective of understanding and capturing physical effects. In this thesis, these models are referred to as simple equivalent-circuit models (S-ECM). Typically, S-ECMs correlate well

with the measured parameters in a limited aspect. In some devices, this may be seen as a good match in low-frequency regions, with a deviation at higher frequencies. In others, only low-order characteristics are captured and the higher-order portion of the response is missed. S-ECMs for various types of devices, such as vias, spiral inductors, small-signal models of transistors, etc., can be found in the literature [1–7].

Capturing these omitted characteristics, even for the most simple structures and devices, becomes extremely difficult [8, 9]. To improve the response of the model, ad-hoc approaches are tried by the designers. These approaches generally involve isolating some physical characteristic or phenomenon that is responsible for the omitted part of the response. Once this is done, the effect is translated into some equivalent circuit elements and added to the S-ECM [1–6, 10]. These approaches can yield good results, but have the following major drawbacks:

1. The correction applies only to a certain type of device that has a similar structure. For example, the correction effected to S-ECMs of spiral inductors may not be valid for a via structure.

2. A large amount of trial-and-error may be required to determine the best location, best structure (resistor, capacitor, etc.), best connection (series or parallel) and the optimum values of the new circuit elements.

3. As the S-ECM complexity is increased, the model correction process may be-

come complicated and turn into a non-linear optimization problem, resulting in excessive computational complexity.

To handle the above difficulties, recently, black-box (or purely mathematical) modelling algorithms based on passive macromodelling have emerged in the literature [11, 12]. However, due to the black-box nature of the process, passivity enforcement can be a time-consuming process. Also, the physical intuitiveness of the device under consideration is completely lost in these models. This is a major concern for the designers who are accustomed to optimizing certain parameters of the S-ECM (and consequently, the physical device) to meet the design specifications.

Hence, it is necessary to develop an algorithm that can retain the S-ECM while providing some augmenting network to address the error. The algorithm in [8, 9] considers such an approach where the S-ECM is augmented with a black-box model so as to match the y-parameters of the S-ECM with the given measured parameters. It was based on finding the augmenting network by curve-fitting the difference between the given measured parameters and that of the S-ECM. One of the drawbacks of this approach is that the augmented network is restricted in its placement to be only at the terminals of the S-ECM. This may not be the optimum solution from the perspective of reducing the error. Also, as with any black-box type model, it can become a challenge to ensure passivity, especially with multi-port networks [12, 13].

In order to address the above difficulties, this thesis presents an efficient and

automated algorithm to identify an augmenting equivalent circuit to improve the accuracy of the S-ECM over a frequency range of interest. The algorithm is not restricted in its placement of new elements only to the ports of the S-ECM. On the other hand, it can automatically identify and insert frequency-dependent elements of both types, series and parallel, at any arbitrary location in the S-ECM, as per the requirements of the problem. To match the S-ECM's response to a measured set of y-parameters, the algorithm determines the single-port driving-point impedance for each of these frequency-dependent elements. This is done using a linear formulation (without resorting to any nonlinear optimization). As each element is represented by a single-port network, ensuring its passivity is easy [13]. These networks can be synthesized as passive equivalent circuits [10, 14, 15]. The final (corrected) model, obtained as a result of the algorithm, is referred to as the augmented equivalent circuit model (A-ECM). The proposed method enables the designers to retain their existing physical models while providing a means to capture the high-frequency effects accurately. In addition, the method is very fast as the computations are done using the simplified linear relations developed in this thesis.

1.2 Contributions

The major subject of this thesis is the improvement of equivalent-circuit models of any device. The algorithm presented provides an automated and efficient means to

develop appropriate augmentations to add to an equivalent-circuit model in order to improve its response. The main contributions of this thesis are as follows.

1. An efficient algorithm is developed to determine an appropriate augmenting network to add to an equivalent-circuit model at any given location to correct errors in its response [16–18]. This method is based on large-scale sensitivity and takes advantage of some characteristics of the modified nodal analysis (MNA) formulation to allow for different augmentation configurations.

2. The algorithm is extended to the case where multiple augmentations are added simultaneously [16, 18]. This is done without resorting to nonlinear optimization.

3. The method is then applied to develop accurate lumped models for transmission lines with frequency-dependent parameters [18, 19]. These models have the advantage of being useful in both time- and frequency-domain simulations.

4. Finally, the above model is extended to the case of multiple coupled transmission lines [19].

1.3 Organization of the Thesis

The thesis is organized as follows. Chapter 2 gives a literature survey and background on the methods the work in the thesis is based on. Chapter 3 describes the development of the augmentation algorithm as it applies to general model structures. Some numerical examples from different domains of application are also presented. Chapter 4 describes the development of the lumped model for transmission lines with frequency-dependent parameters. This covers both the single line and multiple coupled line cases. An example for each of these cases is given. Chapter 5 discusses some of the various implementation issues that must be considered while using the proposed algorithm. Finally, Chapter 6 gives a brief summary of the thesis and provides some ideas for future related research.

Chapter 2

Background

2.1 Introduction

Before considering the proposed algorithm of this thesis, an overview of the concepts that are used in its development is useful. First, in Section 2.2, the Modified Nodal Analysis (MNA) formulation of circuit equations is discussed. This formulation is an ideal tool for simulating circuits, and is used for comparing the performance of equivalent-circuit models to measurements done on the modelled devices. Section 2.3 describes methods to quickly determine the effect on a circuit's state when components are changed or added. Finally, Section 2.4 outlines a procedure for converting a single-port network described by a rational function into a physically realizable network.

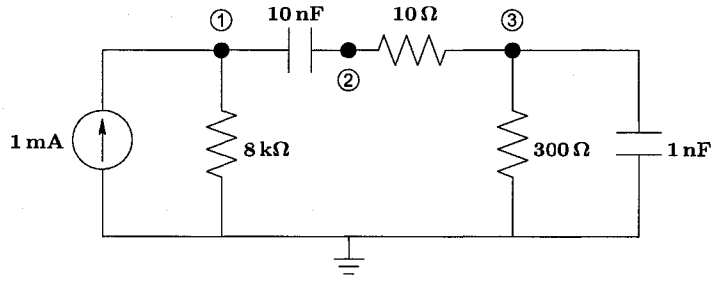

Figure 2.1: Example 1 for Nodal Analysis

2.2 Modified Nodal Analysis

When performing a numerical circuit analysis, an automated means to formulate and solve circuit equations is needed. One such method is Modified Nodal Analysis (MNA) [20]. This has been derived from a standard nodal analysis formulation with various changes for numerical stability and to improve its suitability for implementation in software. Throughout this thesis, this is the method used to analyze the equivalent-circuit models under consideration. The details of this method and how it is derived are described in this section.

To introduce the nodal analysis formulation, consider the example in Figure 2.1. Formulating the nodal equations using Kirchhoff's Current Law (KCL) in the Laplace domain, gives the following.

$$\frac{V_1}{8\times 10^3} + (V_1 - V_2)(10^{-8}s) = 10^{-3} \quad (2.1)$$

$$(V_2 - V_1)(10^{-8}s) + \frac{V_2 - V_3}{10} = 0 \quad (2.2)$$

$$\frac{V_3 - V_2}{10} + \frac{V_3}{300} + V_3(10^9 s) = 0 \quad (2.3)$$

Rewriting this system in matrix form gives

$$\left(\begin{bmatrix} \frac{1}{8\times 10^3} & 0 & 0 \\ 0 & \frac{1}{10} & -\frac{1}{10} \\ 0 & -\frac{1}{10} & \frac{1}{10}+\frac{1}{300} \end{bmatrix} + s \begin{bmatrix} 10^{-8} & -10^{-8} & 0 \\ -10^{-8} & 10^{-8} & 0 \\ 0 & 0 & 10^{-9} \end{bmatrix} \right) \begin{bmatrix} V_1 \\ V_2 \\ V_3 \end{bmatrix} = \begin{bmatrix} 10^{-3} \\ 0 \\ 0 \end{bmatrix} \quad (2.4)$$

Examining these matrices, the following observations are made:

1. The first matrix contains elements related to the conductance of the resistors in the network. Thus, it is called $\boldsymbol{G}$, after the standard symbol for conductance.

2. The second matrix contains elements related to the capacitors in the network. Thus, it is called $\boldsymbol{C}$, for the symbol for capacitance.

3. The combination of $\boldsymbol{G} + s\boldsymbol{C}$ is referred to as the nodal admittance matrix.

4. The vector on the left-hand side contains the nodal voltages of the model. It is identified as $\boldsymbol{v}$.

5. The vector on the right-hand side contains the currents being injected or drawn from the nodes. It will be represented by $\boldsymbol{b}$, from the standard linear

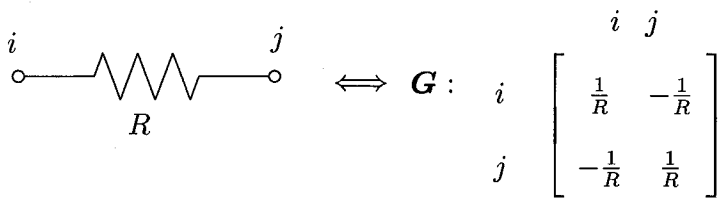

Figure 2.2: Stamp of a Resistor

system form $\boldsymbol{Ax} = \boldsymbol{b}$.

From these observations, the system can be written concisely as

$$(\boldsymbol{G} + s\boldsymbol{C})\boldsymbol{v} = \boldsymbol{b} \tag{2.5}$$

The size of each of these matrices and vectors is dictated by the number of nodes in the circuit. For a system with n nodes $\boldsymbol{G} \in \Re^{n\times n}$, $\boldsymbol{C} \in \Re^{n\times n}$, $\boldsymbol{v} \in \Re^{n}$ and $\boldsymbol{b} \in \Re^{n}$. The next observation is that each element produces a pattern in these matrices that is the same for all elements of a given type. These patterns are called *stamps*. For the elements used in Figure 2.1, the stamps are presented in Figures 2.2, 2.3, and 2.4. A special case for each of these is when one terminal of the device is connected to ground. In this case j is set to zero, and the corresponding row and column from the stamp is omitted. Using these stamps, the contents of all the matrices and vectors can be determined without performing a traditional manual nodal analysis to obtain the system equations.

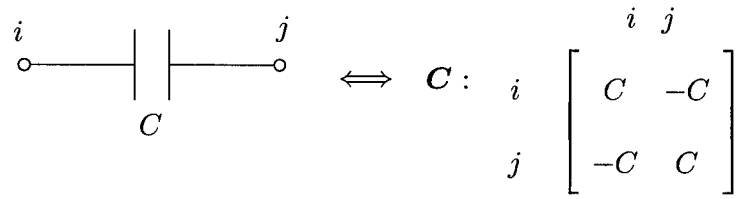

Figure 2.3: Stamp of a Capacitor

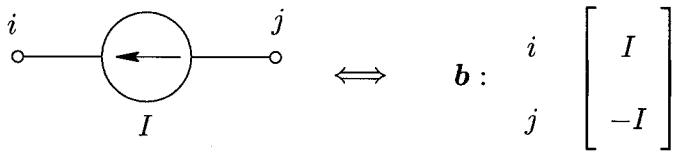

Figure 2.4: Stamp of an Independent Current Source

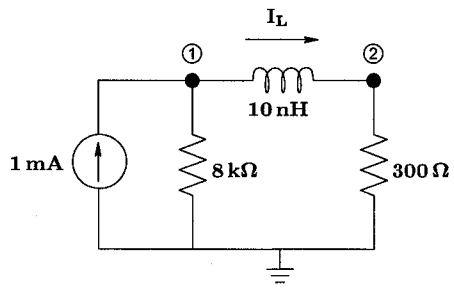

Figure 2.5: Example 2 for Nodal Analysis

The next common circuit element to consider is the inductor. Consider the simple example in Figure 2.5. Performing the nodal analysis as before results in the following system of equations.

$$\frac{V_1}{8 \times 10^3} + \frac{V_1 - V_2}{s10^{-8}} = 10^{-3} \tag{2.6}$$

$$\frac{V_2 - V_1}{s10^{-8}} + \frac{V_2}{300} = 0 \tag{2.7}$$

Rewriting this in matrix form gives the following system.

$$\left(\begin{bmatrix} \frac{1}{8\times10^3} & 0 \\ 0 & \frac{1}{300} \end{bmatrix} + \frac{1}{s} \begin{bmatrix} \frac{1}{10^{-8}} & -\frac{1}{10^{-8}} \\ -\frac{1}{10^{-8}} & \frac{1}{10^{-8}} \end{bmatrix} \right) \begin{bmatrix} V_1 \\ V_2 \end{bmatrix} = \begin{bmatrix} 10^{-3} \\ 0 \end{bmatrix} \tag{2.8}$$

It is observed that the inductor results in a new matrix term corresponding to $\frac{1}{s}$. Although this is mathematically correct, there is a significant disadvantage with this formulation. As the frequency of operation approaches DC, or as $j\omega \rightarrow 0 \Rightarrow s \rightarrow 0$, the $\frac{1}{s}$ term will approach infinity and the system will not have a solution. An alternate way to visualize this problem is to consider that this formulation relies on the admittance of each element. At steady-state DC, an inductor will behave as a

short circuit, so its admittance approach infinity. To avoid this problem, the current through the inductor, I_L, is introduced as a new variable. The circuit equations are reformulated in terms of this variable instead of the inductor characteristics.

$$\frac{V_1}{8 \times 10^3} + I_L = 10^{-3} \tag{2.9}$$

$$-I_L + \frac{V_2}{300} = 0 \tag{2.10}$$

To complete the system, an equation is needed to relate I_L to the behaviour of the inductor. This is clearly given by the following.

$$V_1 - V_2 = 10^{-8} s I_L \tag{2.11}$$

Reformulating these three equations into matrix form gives the following.

$$\left(\begin{bmatrix} \frac{1}{8\times10^3} & 0 & 1 \\ 0 & \frac{1}{300} & -1 \\ 1 & -1 & 0 \end{bmatrix} + s \begin{bmatrix} 0 & 0 & 0 \\ 0 & 0 & 0 \\ 0 & 0 & -10^{-8} \end{bmatrix} \right) \begin{bmatrix} V_1 \\ V_2 \\ I_L \end{bmatrix} = \begin{bmatrix} 10^{-3} \\ 0 \\ 0 \end{bmatrix} \tag{2.12}$$

With the introduction of the extra variable I_L, the term dependent on $\frac{1}{s}$ has been replaced with one proportional to s. Therefore, this new system has a solution for all frequencies. This formulation takes a similar form as the previous nodal admittance form with one important distinction. In this case, the vector of system variables contains not only node voltages but also a branch current. Thus, it is not a true nodal analysis. It is for this reason that this formulation is called Modified Nodal Analysis [20]. The combination of $\boldsymbol{G} + s\boldsymbol{C}$ is now known as the modified nodal

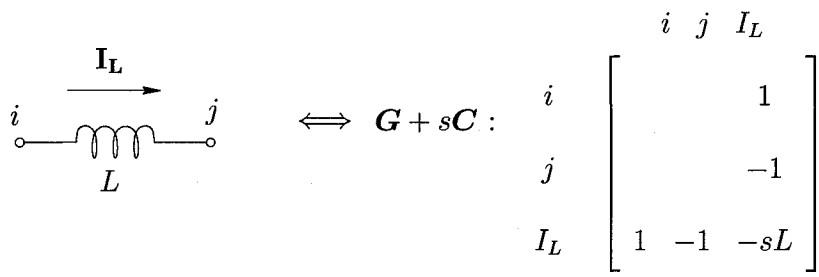

Figure 2.6: MNA Stamp of an Inductor

admittance matrix and is represented by $\boldsymbol{A}$. The vector of system variables is denoted $\boldsymbol{x}$ to reinforce the fact that it can contain variables other than voltages. This new system is given by

$$\boldsymbol{A}\boldsymbol{x} = \boldsymbol{b} \tag{2.13}$$

The MNA stamp for an inductor element as used in the example is shown in Figure 2.6.

The final element to consider is an independent voltage source. For this element, there is no direct relation between its current and voltage. Therefore, a variable for its current needs to be added to allow for a nodal analysis. Consider the example in Figure 2.7. The nodal equations are developed as

$$\frac{V_1}{8 \times 10^3} + (V_1 - V_2)(10^{-8}s) + I_E = 0 \tag{2.14}$$

$$(V_2 - V_1)(10^{-8}s) + \frac{V_2 - V_3}{10} = 0 \tag{2.15}$$

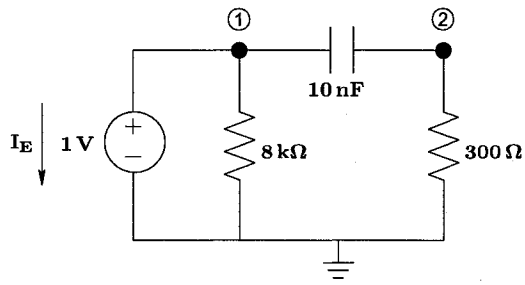

Figure 2.7: Example 3 for Nodal Analysis

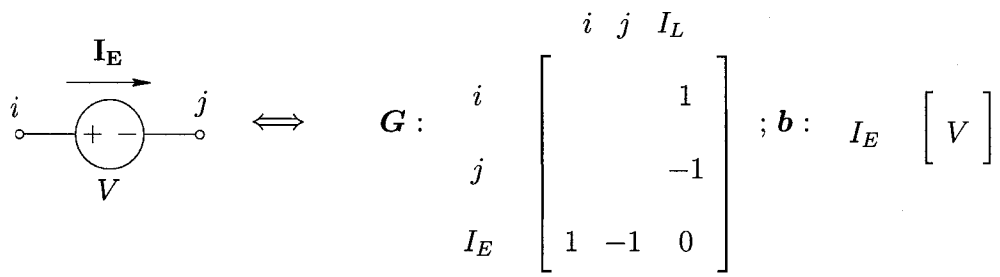

Figure 2.8: MNA Stamp of an Independent Voltage Source

For the third equation, the behaviour of the voltage source is defined.

$$V_1 = 1 \tag{2.16}$$

In matrix form, these equations become

$$\left(\begin{bmatrix} \frac{1}{8\times10^3} & 0 & 1 \\ 0 & \frac{1}{300} & 0 \\ 1 & 0 & 0 \end{bmatrix} + s \begin{bmatrix} 10^{-8} & -10^{-8} & 0 \\ -10^{-8} & 10^{-8} & 0 \\ 0 & 0 & 0 \end{bmatrix} \right) \begin{bmatrix} V_1 \\ V_2 \\ I_E \end{bmatrix} = \begin{bmatrix} 0 \\ 0 \\ 1 \end{bmatrix} \tag{2.17}$$

From this, it is seen that the stamp of a voltage stamp is as given in Figure 2.8.

In the remainder of this thesis, all MNA formulations will be for multi-port net-

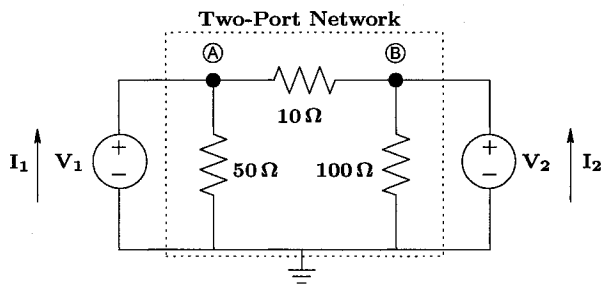

Figure 2.9: Example Two-port Network for MNA

works. As will be seen, it is required that these systems be easily converted into a set of y-parameters for comparison to measured data. By imposing some restrictions on the structure of the network without restricting generality, this can be assured. First, a voltage source excitation is connected to each port. Next, the voltage source stamp is redefined to correspond to the conventional current direction of a multi-port network. These are illustrated by the example in Figure 2.9. Here, it is seen that the direction of the current points into the port as is the convention. However, as seen in Figure 2.8, the direction of the current in the stamp is defined as flowing from the positive terminal to the negative terminal. To compensate for this, a new stamp for a port voltage is presented in Figure 2.10.

Taking advantage of this new stamp along with the resistor stamp in Figure 2.2,

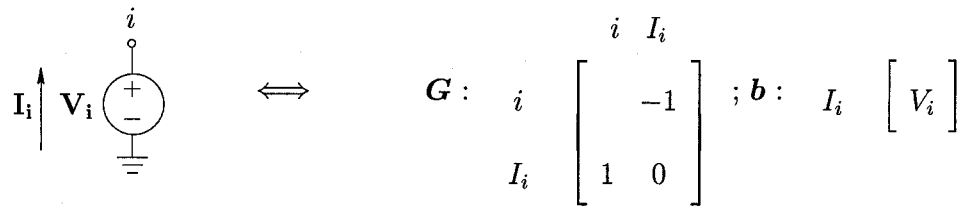

Figure 2.10: MNA Stamp of a Port Voltage Source

the following MNA system is constructed.

$$\begin{bmatrix} \frac{1}{50}+\frac{1}{10} & -\frac{1}{10} & -1 & 0 \\ -\frac{1}{10} & \frac{1}{100}+\frac{1}{10} & 0 & -1 \\ 1 & 0 & 0 & 0 \\ 0 & 1 & 0 & 0 \end{bmatrix} \begin{bmatrix} V_A \\ V_B \\ I_1 \\ I_2 \end{bmatrix} = \begin{bmatrix} 0 \\ 0 \\ V_1 \\ V_2 \end{bmatrix} \tag{2.18}$$

The port voltages can be separated from the $\boldsymbol{b}$ vector by defining a mapping matrix $\boldsymbol{B}$ such that

$$\boldsymbol{b} = \boldsymbol{B} \begin{bmatrix} V_1 \\ V_2 \end{bmatrix} = \boldsymbol{B}\boldsymbol{v} \tag{2.19}$$

Substituting this in (2.13) gives the system

$$\boldsymbol{A}\boldsymbol{x} = \boldsymbol{B}\boldsymbol{v} \tag{2.20}$$

For this example, it is clear that

$$\boldsymbol{B} = \begin{bmatrix} 0 & 0 \\ 0 & 0 \\ 1 & 0 \\ 0 & 1 \end{bmatrix} \tag{2.21}$$

It is observed that this same selector matrix can be used to separate the port currents, I_1 and I_2, from the $\boldsymbol{x}$ vector. The port currents, $\boldsymbol{i}$ are given by

$$\boldsymbol{i} = \boldsymbol{B}^{\mathrm{t}}\boldsymbol{x} \tag{2.22}$$

where the superscript t represents the matrix transpose operator. If the system in (2.20) is now solved for $\boldsymbol{x}$ and substituted in (2.22), the following relation between $\boldsymbol{i}$ and $\boldsymbol{v}$ is obtained.

$$\boldsymbol{i} = \boldsymbol{B}^{\mathrm{t}}\boldsymbol{A}^{-1}\boldsymbol{B}\boldsymbol{v} \tag{2.23}$$

It is known that the y-parameters of a network, denoted by $\boldsymbol{Y}$, are defined as

$$\boldsymbol{i} = \boldsymbol{Y}\boldsymbol{v} \tag{2.24}$$

Therefore, the relationship between the MNA system and the y-parameters is established as

$$\boldsymbol{Y} = \boldsymbol{B}^{\mathrm{t}}\boldsymbol{A}^{-1}\boldsymbol{B} \tag{2.25}$$

2.3 Updating a Modified System

In the previous section, an automated method to formulate the circuit equations of a multi-port network was presented. In addition, a method to convert these equations to the y-parameters was shown. When an equivalent-circuit model is being modified or optimized to match a measured set of y-parameters, small changes are being introduced to the circuit. These changes can be small, such as a perturbation of one of its components, or larger, like the addition of a new component. For this optimization, it is desirable to have a method to determine the change to the overall y-parameters of a model due to these modifications. For efficiency, this should be done without reformulating and solving the entire system. In the following sections, methods to accomplish this are presented.

2.3.1 Small-Scale Sensitivity

When a small change is being considered to an existing component in a model, a small-scale method called *adjoint sensitivity* can be used to determine the corresponding effect on the model's behaviour.

Consider the MNA system defined in (2.20). Let ϕ be the value of a component of interest in the model. The effect of changing this element is given by the derivative

of this system with respect to ϕ.

$$\frac{\partial \boldsymbol{A}\boldsymbol{x}}{\partial \phi} = \frac{\partial \boldsymbol{B}\boldsymbol{v}}{\partial \phi} \tag{2.26}$$

As ϕ represents the value of a component, it does not affect the applied port voltages, $\boldsymbol{v}$, or the way these are mapped to the MNA system, given by $\boldsymbol{B}$. Therefore, $\frac{\partial \boldsymbol{B}\boldsymbol{v}}{\partial \phi} = 0$ and

$$\frac{\partial \boldsymbol{A}\boldsymbol{x}}{\partial \phi} = 0 \tag{2.27}$$

Expanding this with the product rule and rearranging gives

$$\frac{\partial \boldsymbol{A}}{\partial \phi}\boldsymbol{x} + \boldsymbol{A}\frac{\partial \boldsymbol{x}}{\partial \phi} = 0 \tag{2.28}$$

$$\boldsymbol{A}\frac{\partial \boldsymbol{x}}{\partial \phi} = -\frac{\partial \boldsymbol{A}}{\partial \phi}\boldsymbol{x} \tag{2.29}$$

$$\frac{\partial \boldsymbol{x}}{\partial \phi} = -\boldsymbol{A}^{-1}\frac{\partial \boldsymbol{A}}{\partial \phi}\boldsymbol{x} \tag{2.30}$$

It is seen that (2.30) gives a relation between the change in the value of the component and the corresponding effect on the MNA variables. With knowledge of the MNA formulation, it is clear that $\frac{\partial \boldsymbol{A}}{\partial \phi}$ is simply the derivative of the component's stamp with respect to the component's value.

Next, define the k^{th} column of $\boldsymbol{B}$ as $\boldsymbol{b}_k$. For an n-port system, this means

$$\boldsymbol{B} = [\boldsymbol{b}_1 \quad \boldsymbol{b}_2 \quad \cdots \quad \boldsymbol{b}_n] \tag{2.31}$$

Combining (2.31) with (2.22), the k^{th} port current can be extracted from $\boldsymbol{x}$.

$$i_k = \boldsymbol{b}_k^{\text{t}}\boldsymbol{x} \tag{2.32}$$

The sensitivity of i_k to changes in ϕ is found as

$$\frac{\partial i_k}{\partial \phi} = \frac{\partial \boldsymbol{b}_k^{\mathrm{t}} \boldsymbol{x}}{\partial \phi} = \boldsymbol{b}_k^{\mathrm{t}} \frac{\partial \boldsymbol{x}}{\partial \phi} \tag{2.33}$$

Substituting in (2.30), this expands to

$$\frac{\partial i_k}{\partial \phi} = -\boldsymbol{b}_k^{\mathrm{t}} \boldsymbol{A}^{-1} \frac{\partial \boldsymbol{A}}{\partial \phi} \boldsymbol{x} \tag{2.34}$$

Let $\boldsymbol{x}_k^{(\mathrm{a})}$ be a solution to what is termed the *adjoint system*, $\boldsymbol{A}^{\mathrm{t}} \boldsymbol{x}_k^{(\mathrm{a})} = -\boldsymbol{b}_k$. Following some manipulations

$$\boldsymbol{A}^{\mathrm{t}} \boldsymbol{x}_k^{(\mathrm{a})} = -\boldsymbol{b}_k \tag{2.35}$$

$$\boldsymbol{x}_k^{(\mathrm{a})} = -\boldsymbol{A}^{-\mathrm{t}} \boldsymbol{b}_k \tag{2.36}$$

$$(\boldsymbol{x}_k^{(\mathrm{a})})^{\mathrm{t}} = \left[-\boldsymbol{A}^{-\mathrm{t}} \boldsymbol{b}_k\right]^{\mathrm{t}} \tag{2.37}$$

$$(\boldsymbol{x}_k^{(\mathrm{a})})^{\mathrm{t}} = -\boldsymbol{b}_k^{\mathrm{t}} \boldsymbol{A}^{-1} \tag{2.38}$$

This result can be substituted in (2.34) to obtain the following.

$$\frac{\partial i_k}{\partial \phi} = (\boldsymbol{x}_k^{(\mathrm{a})})^{\mathrm{t}} \frac{\partial \boldsymbol{A}}{\partial \phi} \boldsymbol{x} \tag{2.39}$$

Next, this is extended to find the change in all port currents simultaneously.

$$\frac{\partial \boldsymbol{i}}{\partial \phi} = \begin{bmatrix} \frac{\partial i_1}{\partial \phi} \\ \frac{\partial i_2}{\partial \phi} \\ \vdots \\ \frac{\partial i_n}{\partial \phi} \end{bmatrix} = \begin{bmatrix} (\boldsymbol{x}_1^{(\mathrm{a})})^{\mathrm{t}} \frac{\partial \boldsymbol{A}}{\partial \phi} \boldsymbol{x} \\ (\boldsymbol{x}_2^{(\mathrm{a})})^{\mathrm{t}} \frac{\partial \boldsymbol{A}}{\partial \phi} \boldsymbol{x} \\ \vdots \\ (\boldsymbol{x}_n^{(\mathrm{a})})^{\mathrm{t}} \frac{\partial \boldsymbol{A}}{\partial \phi} \boldsymbol{x} \end{bmatrix} = \begin{bmatrix} (\boldsymbol{x}_1^{(\mathrm{a})})^{\mathrm{t}} \\ (\boldsymbol{x}_2^{(\mathrm{a})})^{\mathrm{t}} \\ \vdots \\ (\boldsymbol{x}_n^{(\mathrm{a})})^{\mathrm{t}} \end{bmatrix} \frac{\partial \boldsymbol{A}}{\partial \phi} \boldsymbol{x} \tag{2.40}$$

Replacing $\boldsymbol{x}$ with the solution of (2.20) gives

$$\frac{\partial \boldsymbol{i}}{\partial \phi} = \begin{bmatrix} (\boldsymbol{x}_1^{(\mathrm{a})})^{\mathrm{t}} \\ (\boldsymbol{x}_2^{(\mathrm{a})})^{\mathrm{t}} \\ \vdots \\ (\boldsymbol{x}_n^{(\mathrm{a})})^{\mathrm{t}} \end{bmatrix} \frac{\partial \boldsymbol{A}}{\partial \phi} \boldsymbol{A}^{-1} \boldsymbol{B} \boldsymbol{v} \tag{2.41}$$

Taking the derivative of (2.24) with respect to ϕ results in the following.

$$\frac{\partial \boldsymbol{i}}{\partial \phi} = \frac{\partial \boldsymbol{Y} \boldsymbol{v}}{\partial \phi} = \frac{\partial \boldsymbol{Y}}{\partial \phi} \boldsymbol{v} + \boldsymbol{Y} \frac{\partial \boldsymbol{v}}{\partial \phi} \tag{2.42}$$

As discussed previously, it is known that $\frac{\partial \boldsymbol{v}}{\partial \phi} = 0$, which implies that

$$\frac{\partial \boldsymbol{i}}{\partial \phi} = \frac{\partial \boldsymbol{Y} \boldsymbol{v}}{\partial \phi} = \frac{\partial \boldsymbol{Y}}{\partial \phi} \boldsymbol{v} \tag{2.43}$$

Comparing (2.41) and (2.43) it becomes clear that

$$\frac{\partial \boldsymbol{Y}}{\partial \phi} = \begin{bmatrix} (\boldsymbol{x}_1^{(\mathrm{a})})^{\mathrm{t}} \\ (\boldsymbol{x}_2^{(\mathrm{a})})^{\mathrm{t}} \\ \vdots \\ (\boldsymbol{x}_n^{(\mathrm{a})})^{\mathrm{t}} \end{bmatrix} \frac{\partial \boldsymbol{A}}{\partial \phi} \boldsymbol{A}^{-1} \boldsymbol{B} \tag{2.44}$$

Therefore, for a small change of ϕ, $\Delta\phi$, the updated y-parameters, $\hat{\boldsymbol{Y}}$, are given by

$$\hat{\boldsymbol{Y}} = \boldsymbol{Y} + \frac{\partial \boldsymbol{Y}}{\partial \phi} \Delta\phi = \boldsymbol{Y} + \begin{bmatrix} (\boldsymbol{x}_1^{(\mathrm{a})})^{\mathrm{t}} \\ (\boldsymbol{x}_2^{(\mathrm{a})})^{\mathrm{t}} \\ \vdots \\ (\boldsymbol{x}_n^{(\mathrm{a})})^{\mathrm{t}} \end{bmatrix} \frac{\partial \boldsymbol{A}}{\partial \phi} \boldsymbol{A}^{-1} \boldsymbol{B} \Delta\phi \tag{2.45}$$

It is noted that the only part of this relation that is dependent on the component being varied is the $\frac{\partial \boldsymbol{A}}{\partial \phi}$ term. Therefore, the remaining terms can be computed once per model and used to determine the effect of varying each component.

2.3.2 Large-Scale Sensitivity

In many cases, a model is being changed more than small-scale sensitivity can handle. An existing component might be changed by a large amount, or new components might be added. In either case, it becomes necessary to employ large-scale sensitivity.

Rohrer's Approach

This approach to large-scale sensitivity was described by Rohrer [21] as a consequence of Kron's method of tearing. The version of the derivation provided here has been slightly modified to correspond to the MNA formulations that will be considered in this thesis, as described in Section 2.2.

This problem is formulated as follows. Consider an m-port network corresponding to a simple equivalent-circuit model (S-ECM). This model contains no independent sources and has a voltage excitation at each port. The Modified Nodal Analysis (MNA) equations can be written in the form described in Section 2.2.

$$\boldsymbol{A}(\jmath\omega)\boldsymbol{x} = \boldsymbol{B}\boldsymbol{v} \tag{2.46}$$

where $\boldsymbol{A}(\jmath\omega) \in \mathbb{C}^{N\times N}$ is the MNA matrix at frequency ω, $\boldsymbol{B} \in \mathbb{R}^{N\times m}$ is a binary

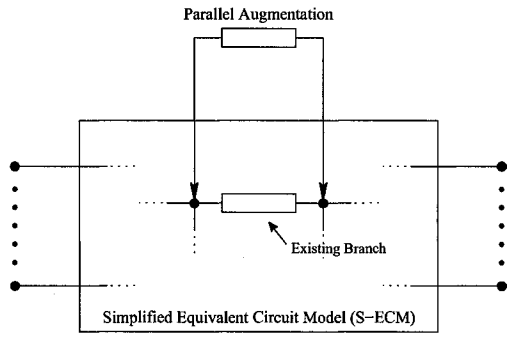

Figure 2.11: Parallel Augmentation

selector matrix which maps the port voltages into the nodal space of the MNA matrix, $\boldsymbol{v} \in \mathbb{C}^{m\times 1}$ is a vector that contains the voltage sources connected to the terminals, and $\boldsymbol{x} \in \mathbb{C}^{N\times 1}$ is a vector containing the unknown MNA variables. From (2.25), the y-parameters of the m-port equivalent circuit can be written as

$$\boldsymbol{Y} = \boldsymbol{B}^{\mathrm{t}}\boldsymbol{A}^{-1}\boldsymbol{B} \tag{2.47}$$

where the superscript t denotes the matrix transpose operator.

Consider the case where an augmentation is being added between two existing nodes in the model. In effect, this is in parallel with an existing set of elements as shown in Figure 2.11 and is termed a *parallel augmentation.* Let v_{oc} represent the open-circuit voltage between these nodes; that is, with no augmentation connected, at a fixed frequency of ω_o. Next, define $\boldsymbol{\xi}$ as an $N \times 1$ selector vector that maps the nodes of the augmenting impedance to the nodal space of the existing MNA in (2.46). For example, when an augmentation is connected between nodes k and l, $\boldsymbol{\xi}$ can be

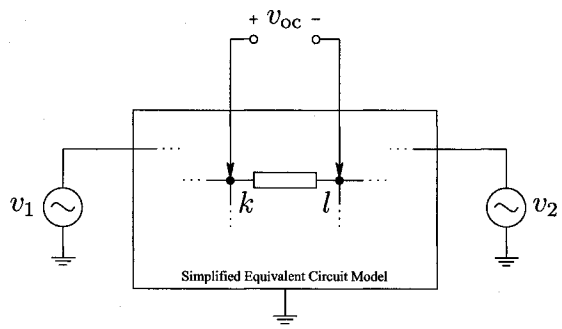

Figure 2.12: Open-circuit voltage between nodes k and l

written as

$$\boldsymbol{\xi} = \begin{bmatrix} \vdots \\ 0 \\ 1 \\ 0 \\ \vdots \\ 0 \\ -1 \\ 0 \\ \vdots \end{bmatrix} \begin{matrix} \\ \\ \longleftarrow k^{\text{th}} \text{ entry} \\ \\ \\ \\ \longleftarrow l^{\text{th}} \text{ entry} \\ \\ \\ \end{matrix} \tag{2.48}$$

For a two-port model, the measurement of v_{oc} is shown in Figure 2.12. The relationship between v_{oc}, $\boldsymbol{\xi}$, and (2.46) can be expressed as

$$v_{\text{oc}} = v_k - v_l = \boldsymbol{\xi}^{\text{t}} \boldsymbol{x}(j\omega_o) = \boldsymbol{\xi}^{\text{t}} \boldsymbol{A}(j\omega_o)^{-1} \boldsymbol{B} \boldsymbol{v} \tag{2.49}$$

Next, the port excitation sources are deactivated and a current source of 1 A at a frequency of ω_o is connected between nodes k and l. This will result in a voltage

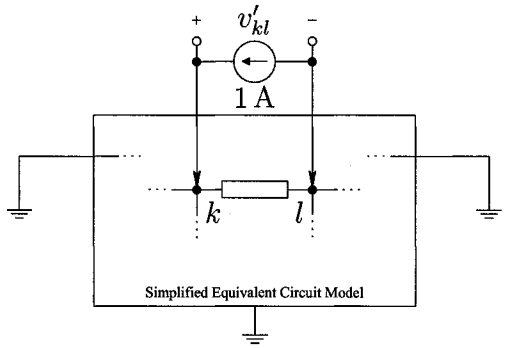

Figure 2.13: Voltage due to a unit current excitation

across these nodes of v'_{kl} as shown in Figure 2.13. Mathematically, this action replaces the relationship in (2.46) with

$$\boldsymbol{A}(j\omega_o)\boldsymbol{x}' = \boldsymbol{\xi} \tag{2.50}$$

where $\boldsymbol{x}'$ represents the new values of the MNA variables under this new excitation. Solving for $\boldsymbol{x}'$ and then v'_{kl} gives

$$\boldsymbol{x}' = \boldsymbol{A}^{-1}\boldsymbol{\xi} \tag{2.51}$$

$$v'_{kl} = v'_k - v'_l = \boldsymbol{\xi}^{\mathrm{t}}\boldsymbol{x}' = \boldsymbol{\xi}^{\mathrm{t}}\boldsymbol{A}^{-1}\boldsymbol{\xi} \tag{2.52}$$

Consider that the nodes k and l form a port to the network. The relation in (2.52) gives the voltage seen at this port given a unit current excitation. This information allows finding the Thévenin equivalent network seen looking in this port. The Thévenin equivalent impedance, z_{th}, is given by

$$z_{\mathrm{th}} = \frac{v'_{kl}}{i} = v'_{kl} = \boldsymbol{\xi}^{\mathrm{t}}\boldsymbol{A}^{-1}\boldsymbol{\xi} \tag{2.53}$$

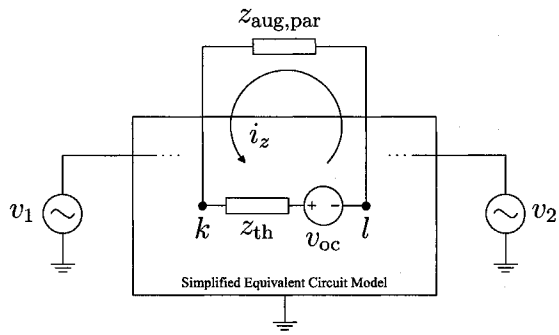

Figure 2.14: Thévenin equivalent circuit of the port connected to nodes k and l

The relations in (2.49) and (2.53) lead to the Thévenin equivalent circuit of this port shown in Figure 2.14. Connecting an impedance of $z_{\text{aug,par}}$ across the port will result in a loop current, i_z, given by

$$i_z = \frac{-v_{\text{oc}}}{z_{\text{aug,par}} + z_{\text{th}}} = \frac{-\boldsymbol{\xi}^{\text{t}}\boldsymbol{A}^{-1}\boldsymbol{B}\boldsymbol{v}}{z_{\text{aug,par}} + \boldsymbol{\xi}^{\text{t}}\boldsymbol{A}^{-1}\boldsymbol{\xi}} \tag{2.54}$$

By the substitution theorem, $z_{\text{aug,par}}$ can be replaced with a current source of i_z without changing the state of the circuit. This results in the circuit shown in Figure 2.15. Next, the new state of the MNA variables in (2.46) after the augmentation is added can be found using superposition.

First, the current source of i_z is considered by itself. From (2.50) and (2.51) it is known that if $i_z = 1$ then $\boldsymbol{x}' = \boldsymbol{A}^{-1}\boldsymbol{\xi}$. Using the linearity theorem, i_z can be scaled to the value in (2.54). This will scale the MNA variables in (2.50) by the same factor. The scaled set of MNA variables is denoted as $\Delta\boldsymbol{x}$ and are given by

$$\Delta\boldsymbol{x} = \frac{-\boldsymbol{\xi}^{\text{t}}\boldsymbol{A}^{-1}\boldsymbol{B}\boldsymbol{v}}{z_{\text{aug,par}} + \boldsymbol{\xi}^{\text{t}}\boldsymbol{A}^{-1}\boldsymbol{\xi}}\boldsymbol{A}^{-1}\boldsymbol{\xi} \tag{2.55}$$

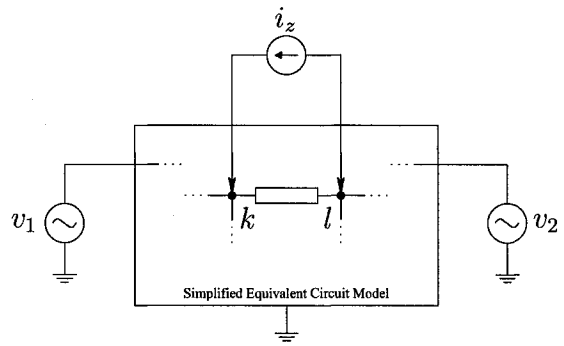

Figure 2.15: Equivalent augmented circuit with substituted current source

Finally, it is noted that when the port voltage sources are considered together and the current source is deactivated, the same circuit as Figure 2.12 is obtained. Therefore, the state of the MNA variables for this case is identical to (2.46), or

$$\boldsymbol{x} = \boldsymbol{A}^{-1}\boldsymbol{B}\boldsymbol{v} \tag{2.56}$$

Combining these two results, the full state of the system is obtained, denoted $\hat{\boldsymbol{x}}$.

$$\hat{\boldsymbol{x}} = \boldsymbol{x} + \Delta\boldsymbol{x} \tag{2.57}$$

or

$$\hat{\boldsymbol{x}} = \boldsymbol{A}^{-1}\boldsymbol{B}\boldsymbol{v} - \boldsymbol{A}^{-1}\boldsymbol{\xi}\frac{\boldsymbol{\xi}^{\mathrm{t}}\boldsymbol{A}^{-1}\boldsymbol{B}\boldsymbol{v}}{z_{\mathrm{aug,par}} + \boldsymbol{\xi}^{\mathrm{t}}\boldsymbol{A}^{-1}\boldsymbol{\xi}} \tag{2.58}$$

Using this result with (2.46) and (2.47), an expression for the changes in the y-parameters due to the augmentation is found as

$$\Delta\boldsymbol{Y} \;=\; \hat{\boldsymbol{Y}} - \boldsymbol{Y} = \frac{-\boldsymbol{B}^{\mathrm{t}}\boldsymbol{A}^{-1}\boldsymbol{\xi}(\boldsymbol{\xi}^{\mathrm{t}}\boldsymbol{A}^{-1}\boldsymbol{B})}{z_{\mathrm{aug,par}} + \boldsymbol{\xi}^{\mathrm{t}}\boldsymbol{A}^{-1}\boldsymbol{\xi}} \tag{2.59}$$

Sherman-Morrison Matrix Inverse Updating

The above result can also be obtained through an alternate formulation based on the Sherman-Morrison formula for updating a matrix inverse [22]. The simplified version of this formula used here was discussed by Householder in [23]. This formulation provides a more mathematical but less intuitive approach than that provided by Rohrer.

When a circuit has a parallel augmentation added as shown in Figure 2.11, the MNA matrix $\boldsymbol{A}$ of (2.46) is modified using the stamp in Figure 2.2. The modified MNA matrix, $\hat{\boldsymbol{A}}$ is given by

$$\hat{\boldsymbol{A}} = \boldsymbol{A} + \boldsymbol{\xi}\boldsymbol{\xi}^{\mathrm{t}} z_{\mathrm{aug,par}}^{-1} \tag{2.60}$$

where $z_{\mathrm{aug,par}}$ is the impedance of the augmentation being added and $\boldsymbol{\xi}$ is the selector vector that describes the augmentation's connection to the circuit, as illustrated in (2.48).

From this, the updated y-parameters, $\hat{\boldsymbol{Y}}$ are found from the relation in (2.47) to be

$$\hat{\boldsymbol{Y}} = \boldsymbol{B}^{\mathrm{t}} \hat{\boldsymbol{A}}^{-1} \boldsymbol{B} = \boldsymbol{B}^{\mathrm{t}} (\boldsymbol{A} + \boldsymbol{\xi}\boldsymbol{\xi}^{\mathrm{t}} z_{\mathrm{aug,par}}^{-1})^{-1} \boldsymbol{B} \tag{2.61}$$

The inverse of $\boldsymbol{A}$ is assumed to have been calculated during a previous analysis. To provide an efficient means to calculate the updated y-parameters, the Sherman-Morrison formula is used to update the matrix inverse. This formula is the follow-

ing [23].

$$(\boldsymbol{B} - \sigma \boldsymbol{u}\boldsymbol{v}^{\mathrm{t}})^{-1} = \boldsymbol{B}^{-1} + (\sigma^{-1} - \boldsymbol{v}^{\mathrm{t}}\boldsymbol{B}^{-1}\boldsymbol{u})^{-1}\boldsymbol{B}^{-1}\boldsymbol{u}\boldsymbol{v}^{\mathrm{t}}\boldsymbol{B}^{-1} \tag{2.62}$$

valid for any $\sigma \neq (\boldsymbol{v}^{\mathrm{t}}\boldsymbol{B}^{-1}\boldsymbol{u})^{-1}$.

To apply this to this case, the following substitutions are made.

$$\boldsymbol{B} \equiv \boldsymbol{A} \tag{2.63}$$

$$\boldsymbol{u} \equiv \boldsymbol{\xi} \tag{2.64}$$

$$\boldsymbol{v} \equiv \boldsymbol{\xi} \tag{2.65}$$

$$\sigma \equiv -z_{\mathrm{aug,par}}^{-1} \tag{2.66}$$

Making these substitutions in (2.62) gives the following relation.

$$(\boldsymbol{A} + z_{\mathrm{aug,par}}^{-1}\boldsymbol{\xi}\boldsymbol{\xi}^{\mathrm{t}})^{-1} = \boldsymbol{A}^{-1} + (-z_{\mathrm{aug,par}} - \boldsymbol{\xi}^{\mathrm{t}}\boldsymbol{A}^{-1}\boldsymbol{\xi})^{-1}\boldsymbol{A}^{-1}\boldsymbol{\xi}\boldsymbol{\xi}^{\mathrm{t}}\boldsymbol{A}^{-1} \tag{2.67}$$

valid for any $z_{\mathrm{aug,par}} \neq -\boldsymbol{\xi}^{\mathrm{t}}\boldsymbol{A}^{-1}\boldsymbol{\xi}$. From the analysis in the previous section, using (2.53), this can be more intuitively stated as being valid for any $z_{\mathrm{aug,par}} \neq -z_{\mathrm{th}}$.

Substituting this result in (2.61), the updated y-parameters become

$$\hat{\boldsymbol{Y}} = \boldsymbol{B}^{\mathrm{t}}\hat{\boldsymbol{A}}^{-1}\boldsymbol{B} = \boldsymbol{B}^{\mathrm{t}}\left[\boldsymbol{A}^{-1} + (-z_{\mathrm{aug,par}} - \boldsymbol{\xi}^{\mathrm{t}}\boldsymbol{A}^{-1}\boldsymbol{\xi})^{-1}\boldsymbol{A}^{-1}\boldsymbol{\xi}\boldsymbol{\xi}^{\mathrm{t}}\boldsymbol{A}^{-1}\right]\boldsymbol{B} \tag{2.68}$$

Expanding (2.68), substituting (2.47), and rearranging gives

$$\hat{\boldsymbol{Y}} = \boldsymbol{B}^{\mathrm{t}}\boldsymbol{A}^{-1}\boldsymbol{B} + \boldsymbol{B}^{\mathrm{t}}(-z_{\mathrm{aug,par}} - \boldsymbol{\xi}^{\mathrm{t}}\boldsymbol{A}^{-1}\boldsymbol{\xi})^{-1}\boldsymbol{A}^{-1}\boldsymbol{\xi}\boldsymbol{\xi}^{\mathrm{t}}\boldsymbol{A}^{-1}\boldsymbol{B} \tag{2.69}$$

$$\hat{\boldsymbol{Y}} = \boldsymbol{Y} + \frac{\boldsymbol{B}^{\mathrm{t}}\boldsymbol{A}^{-1}\boldsymbol{\xi}(\boldsymbol{\xi}^{\mathrm{t}}\boldsymbol{A}^{-1}\boldsymbol{B})}{-z_{\mathrm{aug,par}} - \boldsymbol{\xi}^{\mathrm{t}}\boldsymbol{A}^{-1}\boldsymbol{\xi}} \tag{2.70}$$

$$\Delta\boldsymbol{Y} = \hat{\boldsymbol{Y}} - \boldsymbol{Y} = \frac{-\boldsymbol{B}^{\mathrm{t}}\boldsymbol{A}^{-1}\boldsymbol{\xi}(\boldsymbol{\xi}^{\mathrm{t}}\boldsymbol{A}^{-1}\boldsymbol{B})}{z_{\mathrm{aug,par}} + \boldsymbol{\xi}^{\mathrm{t}}\boldsymbol{A}^{-1}\boldsymbol{\xi}} \tag{2.71}$$

By inspection, it is clear that (2.59) is identical to (2.71).

2.4 Single-Port Network Synthesis

When a network is being optimized to match a certain response, it is often useful that its structure is not constrained. If the network's structure is allowed to change, a much wider variety of responses can be matched. A simple way to allow this is to represent the network as a single-port black box model in the frequency domain instead of as a set of circuit elements. The driving-point impedance of this network can be specified by a rational function. The rational function can then be permuted by a purely mathematical optimization process to achieve the desired response.

After the final rational function is obtained, it must be converted back into a network of circuit elements so that simulations can be carried out easily in both the time and frequency domains. For any passive rational function, there exists a network of R, L and C elements that shares the same driving-point impedance [15]. Methods to determine the appropriate structure exist in literature [14,15] and the method used in this thesis is described here.

Let the driving-point impedance of the single-port network to be synthesized be $Z(s)$ and be of the form

$$Z(s) = \frac{a_0 + a_1 s + a_2 s^2 + \cdots + a_p s^p}{b_0 + b_1 s + b_2 s^2 + \cdots + b_q s^q} \tag{2.72}$$

where $|p-q| \leq 1$. Assume this network is passive and therefore positive real. This implies that

$$\mathrm{Re}\{Z(\jmath\omega)\} \geq 0 \quad \forall \quad \omega \geq 0 \tag{2.73}$$

The first step is to check for poles along the imaginary axis and at $\omega = \infty$. One of the necessary conditions for a rational function to be positive real is that any poles along the imaginary axis must have purely real residues [15]. Knowing this, the partial fraction expansion including the poles of interest is given by

$$Z(s) = sL + \sum_{i=1}^{n} \left(\frac{k_{i,1}}{s+\jmath\omega_i} + \frac{k_{i,2}}{s-\jmath\omega_i} \right) + Z_1(s) \tag{2.74}$$

$$Z(s) = sL + \sum_{i=1}^{n} \frac{k_i s}{s^2+\omega_i^2} + Z_1(s) \tag{2.75}$$

where L is the residue of the pole at infinity, which exists only when $p > q$. When this is the case, $L = \frac{a_p}{b_q}$. The synthesis of the pole/residue terms is achieved with the parallel combination of a capacitor and an inductor. The values of these elements are given by

$$\frac{k_i s}{s^2+\omega_i^2} = sL_i \parallel \frac{1}{sC_i} \tag{2.76}$$

$$= \frac{sL_i}{1+s^2L_iC_i} \tag{2.77}$$

$$\frac{k_i s}{s^2+\omega_i^2} = \frac{C_i^{-1}s}{s^2+(L_iC_i)^{-1}} \tag{2.78}$$

Therefore, $C_i = \frac{1}{k_i}$ and $L_i = \frac{k_i}{\omega_i^2}$. The network resulting from synthesizing these poles is shown in Figure 2.16.

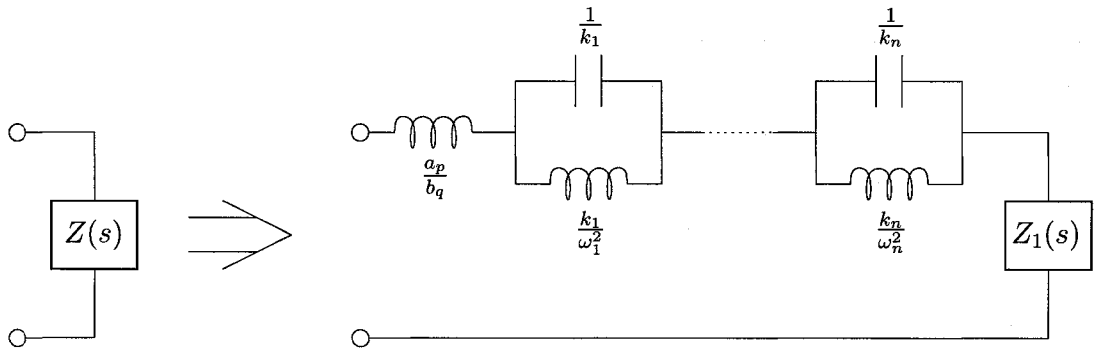

Figure 2.16: Synthesis of Poles on Imaginary Axis

The next step is to synthesize the zeros that occur on the imaginary axis. This can be done in a same way as for the poles along the imaginary axis if it is observed that the zeros of $Z_1(s)$ are the poles of $Y_1(s) = (Z_1(s))^{-1}$. Therefore, the partial fraction expansion can be considered as before

$$Y_1(s) = sC + \sum_{i=1}^{n} \left(\frac{k_{i,1}}{s + j\omega_i} + \frac{k_{i,2}}{s - j\omega_i} \right) + Y_2(s) \tag{2.79}$$

$$Y_1(s) = sC + \sum_{i=1}^{n} \frac{k_i s}{s^2 + \omega_i^2} + Y_2(s) \tag{2.80}$$

where C is the residue of the pole of $Y_1(s)$ at infinity.

The synthesis of the pole/residue terms is achieved with the series combination of a capacitor and an inductor. The values of these elements are given by

$$\frac{k_i s}{s^2 + \omega_i^2} = \frac{1}{sL_i} \parallel sC_i \tag{2.81}$$

$$= \frac{sC_i}{1 + s^2 L_i C_i} \tag{2.82}$$

$$\frac{k_i s}{s^2 + \omega_i^2} = \frac{L_i^{-1} s}{s^2 + (L_i C_i)^{-1}} \tag{2.83}$$

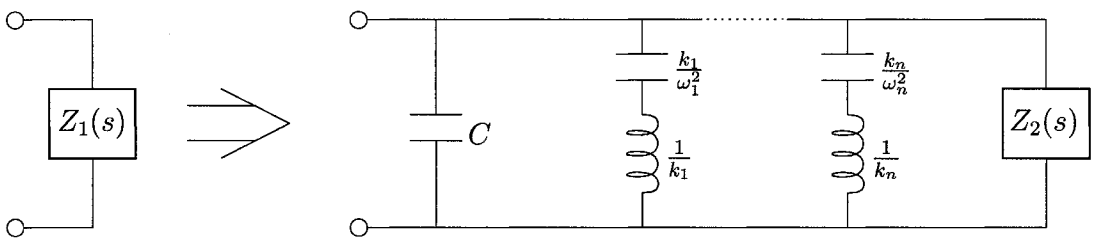

Figure 2.17: Synthesis of Zeros on Imaginary Axis

Therefore, $L_i = \frac{1}{k_i}$ and $C_i = \frac{k_i}{\omega_i^2}$. The network resulting from synthesizing these zeros is shown in Figure 2.17.

At this point the remaining rational function $Z_2(s) = (Y_2(s))^{-1}$ consists only of roots and poles in the left-half plane with no poles or zeros on the imaginary axis and is described by the following form.

$$Z_2(s) = \frac{a_0^{(2)} + a_1^{(2)}s + a_2^{(2)}s^2 + \cdots + a_{p_2}^{(2)}s^{p_2}}{b_0^{(2)} + b_1^{(2)}s + b_2^{(2)}s^2 + \cdots + b_{q_2}^{(2)}s^{q_2}} \tag{2.84}$$

The next task is to extract a series resistance from this function. Let R_1 be the value of this resistance. The maximum value of resistance that can be removed is given by

$$R_1 = \min(\mathrm{Re}\{Z_2(j\omega)\}) \quad , \quad \omega \geq 0 \tag{2.85}$$

If this resistance is removed from $Z_2(s)$ the remainder of the network, $Z_3(s)$, is given by

$$Z_3(s) = Z_2(s) - R_1 \tag{2.86}$$

It is clear that $Z_3(s)$ will be positive real. If $\omega_1 \in \Re, \omega_i \geq 0$ satisfies

$$\mathrm{Re}\{Z_2(\jmath\omega_1)\} = R_1 \tag{2.87}$$

then

$$Z_3(\jmath\omega_1) = \jmath X_1 \tag{2.88}$$

In the case where $\omega_1 = 0$, it can be seen from (2.72) that $R_1 = \mathrm{Re}\{Z_2(0)\} = Z_2(0) = \frac{a_0^{(2)}}{b_0^{(2)}}$. Therefore, $Z_3(s)$ is found by the following

$$Z_3(s) = \frac{a_0^{(2)} + a_1^{(2)}s + a_2^{(2)}s^2 + \cdots + a_{p_2}^{(2)}s^{p_2}}{b_0^{(2)} + b_1^{(2)}s + b_2^{(2)}s^2 + \cdots + b_{q_2}^{(2)}s^{q_2}} - \frac{a_0^{(2)}}{b_0^{(2)}} \tag{2.89}$$

$$Z_3(s) = \frac{a_1^{(3)}s + a_2^{(3)}s^2 + \cdots + a_{p_2}^{(3)}s^{p_2}}{b_0^{(2)} + b_1^{(2)}s + b_2^{(2)}s^2 + \cdots + b_{q_2}^{(2)}s^{q_2}} \tag{2.90}$$

where

$$a_i^{(3)} = \begin{cases} a_i^{(2)} - \frac{b_i^{(2)}a_0^{(2)}}{b_0^{(2)}} & , \quad i \leq \min\{p_2, q_2\} \\ a_i^{(2)} & , \quad q_2 < i \leq p_2 \\ -\frac{b_i^{(2)}a_0^{(2)}}{b_0^{(2)}} & , \quad p_2 < i \leq q_2 \\ 0 & \quad \text{otherwise} \end{cases} \tag{2.91}$$

It can be seen from (2.90) that $Z_3(0) = \jmath X_1 = 0$. This means that $Z_3(s)$ has a zero at $s = 0$. This can be removed if the $b_0^{(2)}$ coefficient is removed in the denominator, creating a pole at $s = 0$, which will cancel out with the zero. This coefficient can be removed by looking at the equivalent driving-point admittance of $Z_3(s)$, $Y_3(s)$. Let $Y_4(s)$ be the driving-point admittance of the remaining network after $b_0^{(2)}$ is eliminated,

given by

$$Y_3(s) = \frac{b_0^{(2)} + b_1^{(2)}s + b_2^{(2)}s^2 + \cdots + b_{q_2}^{(2)}s^{q_2}}{a_1^{(3)}s + a_2^{(3)}s^2 + \cdots + a_{p_2}^{(3)}s^{p_2}} \tag{2.92}$$

$$Y_4(s) = Y_3(s) - \frac{b_0^{(2)}}{a_1^{(3)}s} \tag{2.93}$$

$$Y_4(s) = \frac{b_0^{(2)} + b_1^{(2)}s + b_2^{(2)}s^2 + \cdots + b_{q_2}^{(2)}s^{q_2}}{a_1^{(3)}s + a_2^{(3)}s^2 + \cdots + a_{p_2}^{(3)}s^{p_2}} - \frac{b_0^{(2)}}{a_1^{(3)}s} \tag{2.94}$$

$$Y_4(s) = \frac{b_1^{(4)}s + b_2^{(4)}s^2 + \cdots + b_{q_2}^{(4)}s^{q_2}}{a_1^{(3)}s + a_2^{(3)}s^2 + \cdots + a_{p_2}^{(3)}s^{p_2}} \tag{2.95}$$

$$Y_4(s) = \frac{b_1^{(4)} + b_2^{(4)}s + \cdots + b_{q_2}^{(4)}s^{q_2-1}}{a_1^{(3)} + a_2^{(3)}s + \cdots + a_{p_2}^{(3)}s^{p_2-1}} \tag{2.96}$$

where

$$b_i^{(4)} = \begin{cases} b_i^{(2)} - \frac{a_{i+1}^{(3)}b_0^{(2)}}{a_1^{(3)}} & , \quad i \leq \min\{p_2, q_2\} \\ b_i^{(2)} & , \quad p_2 < i \leq q_2 \\ -\frac{a_i^{(3)}b_0^{(2)}}{a_1^{(3)}} & , \quad q_2 < i \leq p_2 \\ 0 & \text{otherwise} \end{cases} \tag{2.97}$$

It is noted that $Z_4(s)$ has had the order of its numerator and denominator reduced by one compared to $Z_2(s)$ through this process. From this result, it is found that

$$Z_2(s) = R_1 + (sL_1 \parallel Z_4(s)) = \frac{a_0^{(2)}}{b_0^{(2)}} + \left(s\frac{a_1^{(3)}}{b_0^{(2)}} \parallel Z_4(s) \right) \tag{2.98}$$

and this synthesis step is illustrated in Figure 2.18. $Z_4(s)$ is then synthesized by restarting this procedure from the beginning.

In the case where $\omega_1 = \infty$, it can be seen from (2.72) that $R_1 = \text{Re}\{Z_2(\infty)\} = Z_2(\infty) = \frac{a_{q_2}^{(2)}}{b_{q_2}^{(2)}}$, which implies that $p_2 \leq q_2$ and $R_1 = 0$ when $p_2 < q_2$. From this, $Z_3(s)$

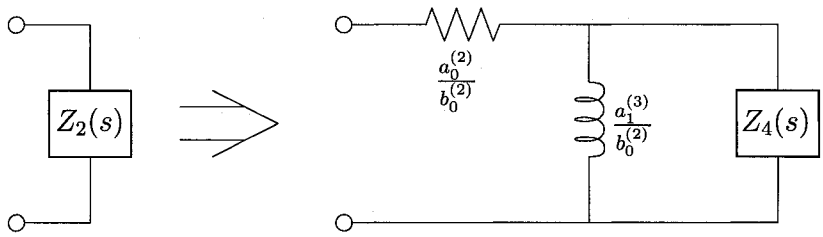

Figure 2.18: Synthesis of minimum resistance at $\omega = 0$

is found to be the following

$$Z_3(s) = \frac{a_0^{(2)} + a_1^{(2)}s + a_2^{(2)}s^2 + \cdots + a_{q_2}^{(2)}s^{q_2}}{b_0^{(2)} + b_1^{(2)}s + b_2^{(2)}s^2 + \cdots + b_{q_2}^{(2)}s^{q_2}} - \frac{a_{q_2}^{(2)}}{b_{q_2}^{(2)}} \tag{2.99}$$

$$Z_3(s) = \frac{a_0^{(3)} + a_1^{(3)}s + a_2^{(3)}s^2 + \cdots + a_{q_2-1}^{(3)}s^{q_2-1}}{b_0^{(2)} + b_1^{(2)}s + b_2^{(2)}s^2 + \cdots + b_{q_2}^{(2)}s^{q_2}} \tag{2.100}$$

where

$$a_i^{(3)} = \begin{cases} a_i^{(2)} - \frac{b_i^{(2)}a_{q_2}^{(2)}}{b_{q_2}^{(2)}} & , \quad i \leq q_2 - 1 \\ 0 & \text{otherwise} \end{cases} \tag{2.101}$$

It can be seen from (2.100) that $Z_3(\infty) = jX_1 = 0$. This means that $Z_3(s)$ has a zero at $s = \infty$. This can be removed if the $b_{q_2}^{(2)}$ coefficient is removed in the denominator, creating a pole at $s = \infty$, which will cancel out with the zero. This coefficient can be removed by looking at the equivalent driving-point admittance of $Z_3(s)$, $Y_3(s)$. Let $Y_4(s)$ be the driving-point admittance of the remaining network

after $b_{q_2}^{(2)}$ is eliminated, given by

$$Y_3(s) = \frac{b_0^{(2)} + b_1^{(2)}s + b_2^{(2)}s^2 + \cdots + b_{q_2}^{(2)}s^{q_2}}{a_0^{(3)} + a_1^{(3)}s + a_2^{(3)}s^2 + \cdots + a_{q_2-1}^{(3)}s^{q_2-1}} \tag{2.102}$$

$$Y_4(s) = Y_3(s) - \frac{b_{q_2}^{(2)}s}{a_{q_2-1}^{(3)}} \tag{2.103}$$

$$Y_4(s) = \frac{b_0^{(2)} + b_1^{(2)}s + b_2^{(2)}s^2 + \cdots + b_{q_2}^{(2)}s^{q_2}}{a_0^{(3)} + a_1^{(3)}s + a_2^{(3)}s^2 + \cdots + a_{q_2-1}^{(3)}s^{q_2-1}} - \frac{b_{q_2}^{(2)}s}{a_{q_2-1}^{(3)}} \tag{2.104}$$

$$Y_4(s) = \frac{b_0^{(4)} + b_1^{(4)}s + b_2^{(4)}s^2 + \cdots + b_{q_2-1}^{(4)}s^{q_2-1}}{a_0^{(3)} + a_1^{(3)}s + a_2^{(3)}s^2 + \cdots + a_{q_2-1}^{(3)}s^{q_2-1}} \tag{2.105}$$

where

$$b_i^{(4)} = \begin{cases} b_0^{(2)} & , \quad i = 0 \\ b_i^{(2)} - \frac{a_{i-1}^{(3)} b_{q_2}^{(2)}}{a_{q_2-1}^{(3)}} & , \quad 0 < i \leq q_2 - 1 \\ 0 & \text{otherwise} \end{cases} \tag{2.106}$$

It is noted that $Z_4(s)$ has had the order of its numerator and denominator reduced by one compared to $Z_2(s)$ through this process. In the case where $p_2 < q_2$, only the order of the denominator has been reduced by one. In either case, $Z_4(s)$ represents a lower-order system. From this result, it is found that

$$Z_2(s) = R_1 + \left(\frac{1}{sC_1} \parallel Z_4(s)\right) = \frac{a_{q_2}^{(2)}}{b_{q_2}^{(2)}} + \left(\frac{1}{s\frac{b_{q_2}^{(2)}}{a_{q_2-1}^{(3)}}} \parallel Z_4(s)\right) \tag{2.107}$$

and this synthesis step is illustrated in Figure 2.19. $Z_4(s)$ is then synthesized by restarting this procedure from the beginning.

The case where $0 < \omega_1 < \infty$ is more complex, as in this case X_1 is not guaranteed to be 0. Instead, it is synthesized into an inductor.

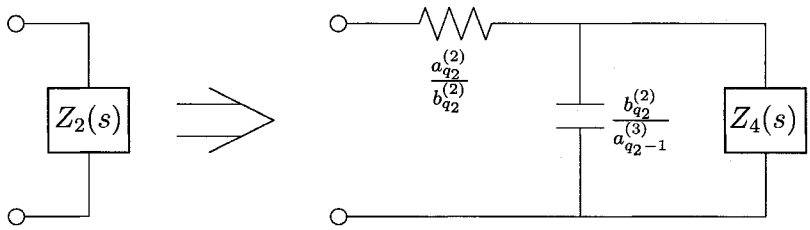

Figure 2.19: Synthesis of minimum resistance at $\omega = \infty$

$$L_1 = \frac{X_1}{\omega_1} \tag{2.108}$$

$$Z_3(s) = sL_1 + Z_4(s) \tag{2.109}$$

It is noted that L_1 may be negative at this point, but it has been shown in [15] that the final representation will result in physical elements. At this point, it is clear that

$$Z_4(j\omega_1) = Z_3(j\omega_1) - j\omega_1 L_1 = jX_1 - jX_1 = 0 \tag{2.110}$$

which means that $Z_4(s)$ has a zero at $s = j\omega_1$. This implies the presence of another zero at $s = -j\omega_1$. In addition, the above relation creates a pole at infinity in $Z_4(s)$.

The zeros at $s = \pm j\omega_1$ can be removed using the procedure above for a zero along the imaginary axis. The partial fraction expansion of the admittance function can be considered as before

$$Y_4(s) = \frac{ks}{s^2 + \omega_1^2} + Y_5(s) \tag{2.111}$$

The synthesis of the pole/residue term is achieved with the series combination of

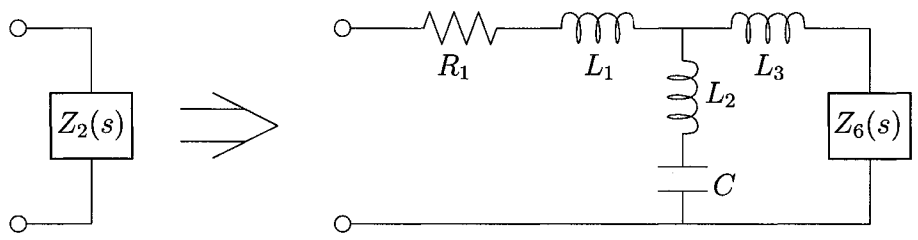

Figure 2.20: Synthesis of minimum resistance at $0 < \omega < \infty$

a capacitor and inductor. The values of these elements are given by

$$\frac{ks}{s^2 + \omega_1^2} = \frac{L_2^{-1}s}{s^2 + (L_2C_1)^{-1}} \tag{2.112}$$

Therefore, $L_2 = \frac{1}{k}$ and $C_1 = \frac{k}{\omega_1^2}$.

Finally, the pole at infinity is removed by the relation

$$Z_5(s) = sL_3 + Z_6(s) \tag{2.113}$$

Figure 2.20 shows the synthesized result of this process. In this structure, a mutual inductance can be seen in its T-model representation. It is possible for a T-model to have negative elements [15] and in this case it is redrawn in its mutual inductance form in Figure 2.21 to ensure its realizability.

Finally, $Z_6(s)$ is synthesized by restarting this procedure from the beginning.

2.5 Summary

In this chapter, some background into numerical methods for circuit analysis was presented. These methods permit the evaluation of the performance of a model and

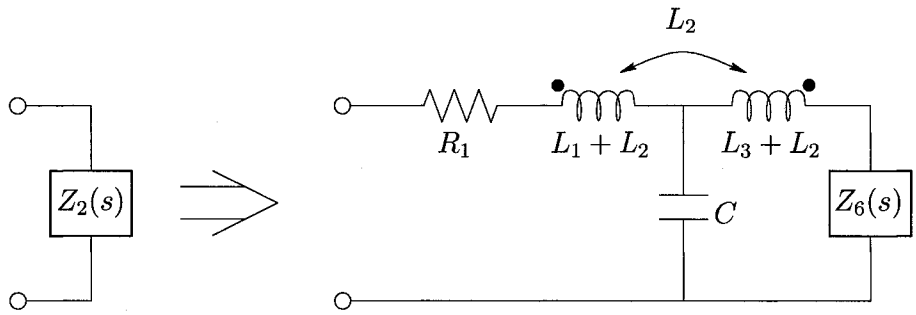

Figure 2.21: Synthesis of minimum resistance at $0 < \omega < \infty$ with mutual inductance

to compare this performance to measurements taken from an actual device. Methods to allow the model's characteristics to be quickly determined following a change were also shown. The final section described a method to synthesize a single-port network whose driving-point impedance is given by a rational function. In the next chapter, this knowledge will be used to develop the proposed algorithm.

Chapter 3

Automated Augmentation of Models

3.1 Introduction

In Chapter 1, it was discussed that for most devices, a simple equivalent-circuit model (S-ECM) is available. These models are generally of a low order, and thus are only able to capture the device's characteristics well over a limited frequency range. Previously, improvements to these models were done in a device-specific and ad-hoc manner. This chapter presents an automated and efficient algorithm to improve an ECM to provide a good match with measured characteristics over a wider frequency range or to capture higher order effects.

This chapter is arranged as follows. First, Section 3.2 describes a method to reduce a model's error by determining an appropriate network to add between two existing nodes to improve its performance. Connected in this matter, the network is said to be in parallel. There are cases where an augmentation would be best placed in series with an existing element. The proposed algorithm is extended to this case in Section 3.3. In Section 3.4, the algorithm is further improved by applying it to the case of multiple simultaneous augmentations. With this addition, multiple augmenting networks can be found for the ECM at once. Finally, in Section 3.5, two examples are presented to demonstrate the effectiveness of this proposed algorithm.

3.2 Addition of a Single Parallel Augmentation

When evaluating the performance of an ECM, its response must be compared to the behaviour of the device it models. In this thesis, this is done by comparing the corresponding y-parameters. Let the given measured y-parameters of the device be represented by $\boldsymbol{Y}_{\text{meas}}$. The goal here is to modify the S-ECM such that it matches the entire broadband spectrum as much as possible by adding an augmenting two-terminal network between a pair of specific nodes as shown in Figure 2.11. Let the corresponding new y-parameters be represented by

$$\hat{\boldsymbol{Y}} = \boldsymbol{Y} + \Delta\boldsymbol{Y} \tag{3.1}$$

The objective here is to find a driving-point impedance, $z_{\text{aug,par}}$, for this augmenting network so as to minimize the following error function

$$\epsilon(\jmath\omega) = \|\boldsymbol{Y}_{\text{meas}}(\jmath\omega) - \hat{\boldsymbol{Y}}(\jmath\omega)\| \tag{3.2}$$

or, by substituting in (2.47) and (3.1),

$$\epsilon(\jmath\omega) = \left\|\boldsymbol{Y}_{\text{meas}}(\jmath\omega) - \boldsymbol{B}^{\text{t}}\boldsymbol{A}^{-1}\boldsymbol{B} - \Delta\boldsymbol{Y}(\jmath\omega)\right\| \tag{3.3}$$

Substituting in (2.59) gives

$$\epsilon(\jmath\omega) = \left\|\boldsymbol{Y}_{\text{meas}}(\jmath\omega) - \boldsymbol{B}^{\text{t}}\boldsymbol{A}^{-1}\boldsymbol{B} + \frac{\boldsymbol{B}^{\text{t}}\boldsymbol{A}^{-1}\boldsymbol{\xi}(\boldsymbol{\xi}^{\text{t}}\boldsymbol{A}^{-1}\boldsymbol{B})}{z_{\text{aug,par}} + \boldsymbol{\xi}^{\text{t}}\boldsymbol{A}^{-1}\boldsymbol{\xi}}\right\| \tag{3.4}$$

In (3.4), all of the terms on the right-hand side are constants at each sampled frequency point except for $z_{\text{aug,par}}$. Therefore, the error is minimized when $z_{\text{aug,par}}$ is the optimal solution, in the least-squares sense, to the over-determined system

$$\left[\boldsymbol{Y}_{\text{meas}}(\jmath\omega) - \boldsymbol{B}^{\text{t}}\boldsymbol{A}^{-1}\boldsymbol{B}\right] z_{\text{aug,par}} = \boldsymbol{B}^{\text{t}}\boldsymbol{A}^{-1}\boldsymbol{\xi}(\boldsymbol{\xi}^{\text{t}}\boldsymbol{A}^{-1}\boldsymbol{B}) - (\boldsymbol{Y}_{\text{meas}}(\jmath\omega) - \boldsymbol{B}^{\text{t}}\boldsymbol{A}^{-1}\boldsymbol{B})\boldsymbol{\xi}^{\text{t}}\boldsymbol{A}^{-1}\boldsymbol{\xi} \tag{3.5}$$

A value for $z_{\text{aug,par}}$ is found with (3.5) at each frequency point. The full response is fit to a rational function with a method such as direct coefficient fit or vector fit as described in Section 5.3 and its passivity is enforced [13]. Finally, the network in synthesized with passive elements with the method of Section 2.4 and inserted into the model. Once this is done, the resulting model is referred to as the augmented equivalent-circuit model (A-ECM).

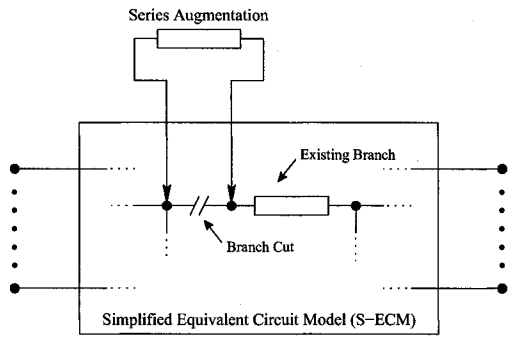

Figure 3.1: Series Augmentation

3.3 Addition of a Single Series Augmentation

In some cases, a parallel augmentation may not be optimal when the passivity constraints are considered. Instead of connecting the augmentation between two existing nodes, it can instead be inserted in series with an existing element, as shown in Figure 3.1. In this section, the algorithm is extended to handle this case.

Consider first the case where the augmentation is a single inductor. When adding this element, the MNA matrix $\boldsymbol{A}$ is updated with the stamp shown in Figure 2.6. This adds two variables to the MNA system. The first corresponds to the new node created by inserting the inductor and the second is for the current through the inductor, I_L.

It is noted that the value in the diagonal of $\boldsymbol{A}$ that corresponds to I_L is equivalent to $-z_{\text{aug,ser}}$, where $z_{\text{aug,ser}} = sL$ is the impedance of the augmenting inductor. Therefore, this stamp can be extended to the general case of an augmenting impedance with the form shown in Figure 3.2.

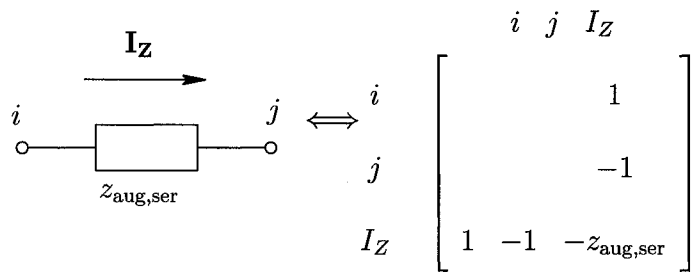

Figure 3.2: MNA Stamp of General Impedance

The goal is to find the value of the augmenting impedance, so the value of $z_{\text{aug,ser}}$ is initially unknown. However, if $z_{\text{aug,ser}}$ is set to zero, the augmentation becomes a short circuit and can be added without affecting the performance of the original S-ECM. If the algorithm can be used to find an appropriate value for the diagonal of $\boldsymbol{A}$ corresponding to I_Z, then it can be used to find the best impedance for the augmentation.

Fortunately, this is possible. It is known that connecting an augmenting impedance of $z_{\text{aug,par}}$ between a given node m and ground causes a value of $z_{\text{aug,par}}^{-1}$ to be added to the m^{th} diagonal of the $\boldsymbol{A}$ matrix. Therefore, if I_Z is on the n^{th} row of $\boldsymbol{x}$, $\boldsymbol{\xi}$ is set to:

$$\boldsymbol{\xi} = \begin{bmatrix} \vdots \\ 0 \\ 1 \\ 0 \\ \vdots \end{bmatrix} \longleftarrow n^{\text{th}} \text{ entry} \tag{3.6}$$

Carrying out the rest of the algorithm as described in the previous section, it will determine the optimal value for $z_{\text{aug,par}}$. This will result in the m^{th} diagonal being set to $z_{\text{aug,par}}^{-1}$. From Figure 3.2, this implies that $z_{\text{aug,ser}} = -z_{\text{aug,par}}^{-1}$. Therefore, (3.5) is modified for the series augmentation case as follows:

$$\left[\boldsymbol{B}^{\text{t}}\boldsymbol{A}^{-1}\boldsymbol{B} - \boldsymbol{Y}_{\text{meas}}(\jmath\omega)\right] z_{\text{aug,ser}}^{-1} = \boldsymbol{B}^{\text{t}}\boldsymbol{A}^{-1}\boldsymbol{\xi}(\boldsymbol{\xi}^{\text{t}}\boldsymbol{A}^{-1}\boldsymbol{B}) - (\boldsymbol{Y}_{\text{meas}}(\jmath\omega) - \boldsymbol{B}^{\text{t}}\boldsymbol{A}^{-1}\boldsymbol{B})\boldsymbol{\xi}^{\text{t}}\boldsymbol{A}^{-1}\boldsymbol{\xi} \tag{3.7}$$

Therefore, the error is minimized when $z_{\text{aug,ser}}$ is the optimal solution, in the least-squares sense, to the over-determined system in (3.7).

Once again, a value for $z_{\text{aug,ser}}$ is found with (3.7) at each frequency point. The full response is fit to a rational function with a method such as those described in Section 5.3 and its passivity is enforced [13]. Finally, the network in synthesized with passive elements as shown in Section 2.4 and inserted into the model, producing the final A-ECM.

3.4 Multiple Simultaneous Augmentations

Many S-ECMs can benefit from the addition of several augmentations at various locations. Up to this point, to accomplish this, the augmentations would have to be found one at a time. In general, this may not lead to fast convergence on the optimal solution. To speed this up, the ability to determine appropriate networks for multiple

simultaneous augmentations and to evaluate their impact on the S-ECM is required. In order to handle these efficiently, simplified linear relations have been developed for this case.

Consider a problem with n_{par} parallel augmentations and n_{ser} series augmentations. Let $\boldsymbol{\xi}_{\text{par},i}$ be the selector vector in the form of (2.48) for the i^{th} parallel augmentation, $z_{\text{aug,par},i}$. Similarly, $\boldsymbol{\xi}_{\text{ser},k}$ is defined as the selector vector in the form of (3.6) for the k^{th} series augmentation, $z_{\text{aug,ser},k}$.

Ordinarily, the total effect of adding multiple augmentations into a model will be different than the sum of the effects. However, assuming that the S-ECM is already a fair representation of the device and the augmentations are being added to refine its response, the higher order coupling terms can be neglected. Thus, the total effect of adding these augmentations on the y-parameters is given by:

$$\Delta \boldsymbol{Y} = \sum_{i=1}^{n_{\text{par}}} \frac{-\boldsymbol{B}^{\text{t}}\boldsymbol{A}^{-1}\boldsymbol{\xi}_{\text{par},i}(\boldsymbol{\xi}_{\text{par},i}^{\text{t}}\boldsymbol{A}^{-1}\boldsymbol{B})}{z_{\text{aug,par},i} + \boldsymbol{\xi}_{\text{par},i}^{\text{t}}\boldsymbol{A}^{-1}\boldsymbol{\xi}_{\text{par},i}} + \sum_{k=1}^{n_{\text{ser}}} \frac{-\boldsymbol{B}^{\text{t}}\boldsymbol{A}^{-1}\boldsymbol{\xi}_{\text{ser},k}(\boldsymbol{\xi}_{\text{ser},k}^{\text{t}}\boldsymbol{A}^{-1}\boldsymbol{B})}{-z_{\text{aug,ser},k}^{-1} + \boldsymbol{\xi}_{\text{ser},k}^{\text{t}}\boldsymbol{A}^{-1}\boldsymbol{\xi}_{\text{ser},k}} \tag{3.8}$$

Substituting this in the error function (3.3) gives

$$\epsilon(\jmath\omega) = \left\| \boldsymbol{Y}_{\text{meas}}(\jmath\omega) - \boldsymbol{B}^{\text{t}}\boldsymbol{A}^{-1}\boldsymbol{B} + \sum_{i=1}^{n_{\text{par}}} \frac{\boldsymbol{B}^{\text{t}}\boldsymbol{A}^{-1}\boldsymbol{\xi}_{\text{par},i}(\boldsymbol{\xi}_{\text{par},i}^{\text{t}}\boldsymbol{A}^{-1}\boldsymbol{B})}{z_{\text{aug,par},i} + \boldsymbol{\xi}_{\text{par},i}^{\text{t}}\boldsymbol{A}^{-1}\boldsymbol{\xi}_{\text{par},i}} + \sum_{k=1}^{n_{\text{ser}}} \frac{\boldsymbol{B}^{\text{t}}\boldsymbol{A}^{-1}\boldsymbol{\xi}_{\text{ser},k}(\boldsymbol{\xi}_{\text{ser},k}^{\text{t}}\boldsymbol{A}^{-1}\boldsymbol{B})}{-z_{\text{aug,ser},k}^{-1} + \boldsymbol{\xi}_{\text{ser},k}^{\text{t}}\boldsymbol{A}^{-1}\boldsymbol{\xi}_{\text{ser},k}} \right\| \tag{3.9}$$

Straightforward minimization of the error function (3.9) leads to a nonlinear optimization problem. Solution of a nonlinear optimization problem is generally computationally expensive, can have problems with local minima, and is not guaranteed to

converge. To convert this to a linear least-squares optimization problem, the following intermediate variables are introduced:

$$\gamma_{\text{aug,par},i} = (z_{\text{aug,par},i} + \boldsymbol{\xi}_i^{\text{t}} \boldsymbol{A}^{-1} \boldsymbol{\xi}_i)^{-1} \tag{3.10}$$

$$\gamma_{\text{aug,ser},k} = (-z_{\text{aug,ser},k}^{-1} + \boldsymbol{\xi}_k^{\text{t}} \boldsymbol{A}^{-1} \boldsymbol{\xi}_k)^{-1} \tag{3.11}$$

Substituting these in (3.9) gives the following error function:

$$\epsilon(\jmath\omega) = \left\| \boldsymbol{Y}_{\text{meas}}(\jmath\omega) - \boldsymbol{B}^{\text{t}} \boldsymbol{A}^{-1} \boldsymbol{B} + \sum_{i=1}^{n_{\text{par}}} \left(\boldsymbol{B}^{\text{t}} \boldsymbol{A}^{-1} \boldsymbol{\xi}_{\text{par},i} (\boldsymbol{\xi}_{\text{par},i}^{\text{t}} \boldsymbol{A}^{-1} \boldsymbol{B}) \right) \gamma_{\text{aug,par},i} + \sum_{k=1}^{n_{\text{ser}}} \left(\boldsymbol{B}^{\text{t}} \boldsymbol{A}^{-1} \boldsymbol{\xi}_{\text{ser},k} (\boldsymbol{\xi}_{\text{ser},k}^{\text{t}} \boldsymbol{A}^{-1} \boldsymbol{B}) \right) \gamma_{\text{aug,ser},k} \right\| \tag{3.12}$$

In (3.12), all of the terms on the right-hand side are constants at each sampled frequency point except for each γ_{aug}. To formulate this as a linear least-squares optimization problem, the following definitions are made:

$$\boldsymbol{\gamma}_{\text{aug}} = \left[\gamma_{\text{aug,par},1} \quad \cdots \quad \gamma_{\text{aug,par},n_{\text{par}}} \quad \gamma_{\text{aug,ser},1} \quad \cdots \quad \gamma_{\text{aug,ser},n_{\text{ser}}} \right]^{\text{t}} \tag{3.13}$$

$$\boldsymbol{F}^{(\text{par},i)} = -\boldsymbol{B}^{\text{t}} \boldsymbol{A}^{-1} \boldsymbol{\xi}_{\text{par},i} (\boldsymbol{\xi}_{\text{par},i}^{\text{t}} \boldsymbol{A}^{-1} \boldsymbol{B}) \tag{3.14}$$

$$\boldsymbol{F}^{(\text{ser},k)} = -\boldsymbol{B}^{\text{t}} \boldsymbol{A}^{-1} \boldsymbol{\xi}_{\text{ser},k} (\boldsymbol{\xi}_{\text{ser},k}^{\text{t}} \boldsymbol{A}^{-1} \boldsymbol{B}) \tag{3.15}$$

$$\Delta \boldsymbol{Y} = \boldsymbol{Y}_{\text{meas}}(\jmath\omega) - \boldsymbol{B}^{\text{t}} \boldsymbol{A}^{-1} \boldsymbol{B} \tag{3.16}$$

In the case of an m-port model, the error in (3.12) is minimized when $\boldsymbol{\gamma}_{\text{aug}}$ is the

optimal solution, in the least-squares sense, to the system

$$\begin{bmatrix} F_{11}^{(\mathrm{par},1)} & \cdots & F_{11}^{(\mathrm{par},n_{\mathrm{par}})} & F_{11}^{(\mathrm{ser},1)} & \cdots & F_{11}^{(\mathrm{ser},n_{\mathrm{ser}})} \\ F_{12}^{(\mathrm{par},1)} & \cdots & F_{12}^{(\mathrm{par},n_{\mathrm{par}})} & F_{12}^{(\mathrm{ser},1)} & \cdots & F_{12}^{(\mathrm{ser},n_{\mathrm{ser}})} \\ \vdots & \ddots & \vdots & \vdots & \ddots & \vdots \\ F_{1m}^{(\mathrm{par},1)} & \cdots & F_{1m}^{(\mathrm{par},n_{\mathrm{par}})} & F_{1m}^{(\mathrm{ser},1)} & \cdots & F_{1m}^{(\mathrm{ser},n_{\mathrm{ser}})} \\ F_{21}^{(\mathrm{par},1)} & \cdots & F_{21}^{(\mathrm{par},n_{\mathrm{par}})} & F_{21}^{(\mathrm{ser},1)} & \cdots & F_{21}^{(\mathrm{ser},n_{\mathrm{ser}})} \\ \vdots & \ddots & \vdots & \vdots & \ddots & \vdots \\ F_{mm}^{(\mathrm{par},1)} & \cdots & F_{mm}^{(\mathrm{par},n_{\mathrm{par}})} & F_{mm}^{(\mathrm{ser},1)} & \cdots & F_{mm}^{(\mathrm{ser},n_{\mathrm{ser}})} \end{bmatrix} \boldsymbol{\gamma}_{\mathrm{aug}} = \begin{bmatrix} \Delta Y_{11} \\ \Delta Y_{12} \\ \vdots \\ \Delta Y_{1m} \\ \Delta Y_{21} \\ \vdots \\ \Delta Y_{mm} \end{bmatrix} \tag{3.17}$$

It is clear that this is a system of m^2 equations with $(n_{\mathrm{par}} + n_{\mathrm{ser}})$ unknowns. This implies that the number of augmentations is limited by the number of ports of the model. For example, for a two-port model, a maximum of four augmentations can be added this way. If the model is symmetric, the situation is worsened, as $Y_{12} = Y_{21}$ so only three augmentations can be added. If more augmentations are added, the system becomes under-determined, and the excess γ_{aug} terms will evaluate to zero, which is unacceptable.

With this method of fitting, each sampled frequency point is considered independently. The rank of the system can be increased if instead the fitting is carried out for all frequency points simultaneously. This can be done if it is assumed that $\gamma_{\mathrm{aug,par},i}$

and $\gamma_{\text{aug,ser},k}$ can be represented as rational functions of the following form:

$$\gamma_{\text{aug,par},i} = \frac{N_{\text{par},i}(s)}{D(s)} = \frac{a_{\text{par},i,p}s^p + \cdots + a_{\text{par},i,0}}{s^q + b_{q-1}s^{q-1} + \cdots + b_0} \tag{3.18}$$

$$\gamma_{\text{aug,ser},k} = \frac{N_{\text{ser},k}(s)}{D(s)} = \frac{a_{\text{ser},k,p}s^p + \cdots + a_{\text{ser},k,0}}{s^q + b_{q-1}s^{q-1} + \cdots + b_0} \tag{3.19}$$

It is noted that the denominators of (3.18) and (3.19) are the same for each augmentation. This form does not require that each γ_{aug} share the same poles; rather, it implies that the denominator is simply the product of the poles for each. Poles which are not needed by a particular γ_{aug} will be cancelled by zeros in the corresponding $N(s)$ and removed at the end of the procedure.

Substituting (3.18) and (3.19) in (3.12) and expanding the error function to cover each of r frequency points gives

$$\epsilon = \sum_{l=1}^{r} \left\| D(\jmath\omega_l)^{-1} \left(\sum_{i=1}^{n_{\text{par}}} \left(\boldsymbol{B}^{\text{t}}\boldsymbol{A}^{-1}\boldsymbol{\xi}_{\text{par},i}(\boldsymbol{\xi}_{\text{par},i}^{\text{t}}\boldsymbol{A}^{-1}\boldsymbol{B}) \right) N_{,\text{par},i}(\jmath\omega_l) + \right. \right.$$
$$\left. \left. \sum_{k=1}^{n_{\text{ser}}} \left(\boldsymbol{B}^{\text{t}}\boldsymbol{A}^{-1}\boldsymbol{\xi}_{\text{ser},k}(\boldsymbol{\xi}_{\text{ser},k}^{\text{t}}\boldsymbol{A}^{-1}\boldsymbol{B}) \right) N_{\text{ser},k}(\jmath\omega_l) \right) + \boldsymbol{Y}_{\text{meas}}(\jmath\omega_l) - \boldsymbol{B}^{\text{t}}\boldsymbol{A}^{-1}\boldsymbol{B} \right\| \tag{3.20}$$

To formulate this as a linear least-squares optimization problem, the following definitions are made:

$$\boldsymbol{\eta} = \left[a_{\text{par},1,0} \ \cdots \ a_{\text{par},1,p} \ a_{\text{par},2,0} \ \cdots \ a_{\text{par},n_{\text{par}},p} \ a_{\text{ser},1,0} \ \cdots \right.$$
$$\left. \cdots \ a_{\text{ser},1,p} \ a_{\text{ser},2,0} \ \cdots \ a_{\text{ser},n_{\text{ser}},p} \ b_0 \ \cdots \ b_{q-1} \right]^{\text{t}} \tag{3.21}$$

$$\boldsymbol{F}^{(\text{par},i)} = -\boldsymbol{B}^{\text{t}}\boldsymbol{A}^{-1}\boldsymbol{\xi}_{\text{par},i}(\boldsymbol{\xi}_{\text{par},i}^{\text{t}}\boldsymbol{A}^{-1}\boldsymbol{B}) \tag{3.22}$$

$$\boldsymbol{F}^{(\text{ser},k)} = -\boldsymbol{B}^{\text{t}}\boldsymbol{A}^{-1}\boldsymbol{\xi}_{\text{ser},k}(\boldsymbol{\xi}_{\text{ser},k}^{\text{t}}\boldsymbol{A}^{-1}\boldsymbol{B}) \tag{3.23}$$

$$\Delta\boldsymbol{Y} = \boldsymbol{Y}_{\text{meas}}(\jmath\omega) - \boldsymbol{B}^{\text{t}}\boldsymbol{A}^{-1}\boldsymbol{B} \tag{3.24}$$

The error in (3.20) is minimized when $\boldsymbol{\eta}$ is the optimal solution, in the least-squares sense, to the system of (3.27), on the following page.

The final step is to determine a function for each z_{aug} from the corresponding γ_{aug}. For the parallel augmentations, a function $D_{z,\text{par},i}(s) = d_{z,\text{par},i,q}s^q + \cdots + d_{z,\text{par},i,0}$ is found that minimizes the error function

$$\epsilon = \left\| \boldsymbol{\xi}_{\text{par},i}^{\text{t}} \boldsymbol{A}^{-1} \boldsymbol{\xi}_{\text{par},i} - \frac{D_{z,\text{par},i}(s)}{N(s)} \right\| \tag{3.25}$$

Similar to the optimization of the entire system, the optimal coefficients are the solution to the following system:

$$\begin{bmatrix} 1 & 0 & -\omega_0^2 & 0 & \cdots & \text{Re}\{(\jmath\omega_0)^q\} \\ 0 & \omega_0 & 0 & -\omega_0^3 & \cdots & \text{Im}\{(\jmath\omega_0)^q\} \\ \vdots & \vdots & \vdots & \vdots & \ddots & \vdots \\ 1 & 0 & -\omega_r^2 & 0 & \cdots & \text{Re}\{(\jmath\omega_r)^q\} \\ 0 & \omega_r & 0 & -\omega_r^3 & \cdots & \text{Im}\{(\jmath\omega_r)^q\} \end{bmatrix} \begin{bmatrix} d_{z,\text{par},i,0} \\ \vdots \\ d_{z,\text{par},i,q} \end{bmatrix} =$$

$$\begin{bmatrix} \text{Re}(\boldsymbol{\xi}_{\text{par},i}^{\text{t}} \boldsymbol{A}(\jmath\omega_0)^{-1} \boldsymbol{\xi}_{\text{par},i} N(\jmath\omega_0)) \\ \text{Im}(\boldsymbol{\xi}_{\text{par},i}^{\text{t}} \boldsymbol{A}(\jmath\omega_0)^{-1} \boldsymbol{\xi}_{\text{par},i} N(\jmath\omega_0)) \\ \vdots \\ \text{Re}(\boldsymbol{\xi}_{\text{par},i}^{\text{t}} \boldsymbol{A}(\jmath\omega_r)^{-1} \boldsymbol{\xi}_{\text{par},i} N(\jmath\omega_r)) \\ \text{Im}(\boldsymbol{\xi}_{\text{par},i}^{\text{t}} \boldsymbol{A}(\jmath\omega_r)^{-1} \boldsymbol{\xi}_{\text{par},i} N(\jmath\omega_r)) \end{bmatrix} \tag{3.26}$$

$$
\begin{bmatrix}
\mathrm{Re}\{F_{11}^{(\mathrm{par},1)}(\omega_0)\} & -\mathrm{Im}\{F_{11}^{(\mathrm{par},1)}(\omega_0)\}\omega_0 & -\mathrm{Re}\{F_{11}^{(\mathrm{par},1)}(\omega_0)\}\omega_0^2 & \cdots & \mathrm{Re}\{F_{11}^{(\mathrm{par},1)}(\omega_0)(\jmath\omega_0)^p\} & \mathbf{0}_{1\times(n_{\mathrm{ser}}+n_{\mathrm{par}}-1)} \\
\mathrm{Im}\{F_{11}^{(\mathrm{par},1)}(\omega_0)\} & \mathrm{Re}\{F_{11}^{(\mathrm{par},1)}(\omega_0)\}\omega_0 & -\mathrm{Im}\{F_{11}^{(\mathrm{par},1)}(\omega_0)\}\omega_0^2 & \cdots & \mathrm{Im}\{F_{11}^{(\mathrm{par},1)}(\omega_0)(\jmath\omega_0)^p\} & \mathbf{0}_{1\times(n_{\mathrm{ser}}+n_{\mathrm{par}}-1)} \\
\vdots & \vdots & \vdots & \vdots & \vdots & \vdots \\
\mathbf{0}_{1\times(n_{\mathrm{par}}-1)} & \mathrm{Im}\{F_{mm}^{(\mathrm{par},n_{\mathrm{par}})}(\omega_r)\} & \mathrm{Re}\{F_{mm}^{(\mathrm{par},n_{\mathrm{par}})}(\omega_r)\}\omega_r & -\mathrm{Im}\{F_{mm}^{(\mathrm{par},n_{\mathrm{par}})}(\omega_r)\}\omega_r^2 & \cdots & \mathrm{Im}\{F_{mm}^{(\mathrm{par},n_{\mathrm{par}})}(\omega_r)(\jmath\omega_r)^p\} & \mathbf{0}_{1\times n_{\mathrm{ser}}} \\
\mathbf{0}_{1\times n_{\mathrm{par}}} & \mathrm{Re}\{F_{11}^{(\mathrm{ser},1)}(\omega_0)\} & -\mathrm{Im}\{F_{11}^{(\mathrm{ser},1)}(\omega_0)\}\omega_0 & -\mathrm{Re}\{F_{11}^{(\mathrm{ser},1)}(\omega_0)\}\omega_0^2 & \cdots & \mathrm{Re}\{F_{11}^{(\mathrm{ser},1)}(\omega_0)(\jmath\omega_0)^p\} & \mathbf{0}_{1\times(n_{\mathrm{ser}}-1)} \\
\vdots & \vdots & \vdots & \vdots & \vdots & \vdots \\
\mathbf{0}_{1\times(n_{\mathrm{ser}}+n_{\mathrm{par}}-1)} & \mathrm{Re}\{F_{mm}^{(\mathrm{ser},n_{\mathrm{ser}})}(\omega_r)\} & -\mathrm{Im}\{F_{mm}^{(\mathrm{ser},n_{\mathrm{ser}})}(\omega_r)\}\omega_r & -\mathrm{Re}\{F_{mm}^{(\mathrm{ser},n_{\mathrm{ser}})}(\omega_r)\}\omega_r^2 & \cdots & \mathrm{Re}\{F_{mm}^{(\mathrm{ser},n_{\mathrm{ser}})}(\omega_r)(\jmath\omega_r)^p\} & \\
\mathbf{0}_{1\times(n_{\mathrm{ser}}+n_{\mathrm{par}}-1)} & \mathrm{Im}\{F_{mm}^{(\mathrm{ser},n_{\mathrm{ser}})}(\omega_r)\} & \mathrm{Re}\{F_{mm}^{(\mathrm{ser},n_{\mathrm{ser}})}(\omega_r)\}\omega_r & -\mathrm{Im}\{F_{mm}^{(\mathrm{ser},n_{\mathrm{ser}})}(\omega_r)\}\omega_r^2 & \cdots & \mathrm{Im}\{F_{mm}^{(\mathrm{ser},n_{\mathrm{ser}})}(\omega_r)(\jmath\omega_r)^p\} &
\end{bmatrix}
$$

$$
\begin{bmatrix}
-\mathrm{Re}\{\Delta Y_{11}(\omega_0)\} & \mathrm{Im}\{\Delta Y_{11}(\omega_0)\}\omega_0 & \cdots & -\mathrm{Re}\{\Delta Y_{11}(\omega_0)(\jmath\omega_0)^{q-1}\} \\
-\mathrm{Im}\{\Delta Y_{11}(\omega_0)\} & -\mathrm{Re}\{\Delta Y_{11}(\omega_0)\}\omega_0 & \cdots & -\mathrm{Im}\{\Delta Y_{11}(\omega_0)(\jmath\omega_0)^{q-1}\} \\
\vdots & \vdots & \ddots & \vdots \\
-\mathrm{Im}\{\Delta Y_{mm}(\omega_r)\} & -\mathrm{Re}\{\Delta Y_{mm}(\omega_r)\}\omega_r & \cdots & -\mathrm{Im}\{\Delta Y_{mm}(\omega_r)(\jmath\omega_r)^{q-1}\} \\
-\mathrm{Re}\{\Delta Y_{11}(\omega_0)\} & \mathrm{Im}\{\Delta Y_{11}(\omega_0)\}\omega_0 & \cdots & -\mathrm{Re}\{\Delta Y_{11}(\omega_0)(\jmath\omega_0)^{q-1}\} \\
\vdots & \vdots & \ddots & \vdots \\
-\mathrm{Re}\{\Delta Y_{mm}(\omega_r)\} & \mathrm{Im}\{\Delta Y_{mm}(\omega_r)\}\omega_r & \cdots & -\mathrm{Re}\{\Delta Y_{mm}(\omega_r)(\jmath\omega_r)^{q-1}\} \\
-\mathrm{Im}\{\Delta Y_{mm}(\omega_r)\} & -\mathrm{Re}\{\Delta Y_{mm}(\omega_r)\}\omega_r & \cdots & -\mathrm{Im}\{\Delta Y_{mm}(\omega_r)(\jmath\omega_r)^{q-1}\}
\end{bmatrix}
\boldsymbol{\eta} =
\begin{bmatrix}
\mathrm{Re}\{\Delta Y_{11}(\omega_0)(\jmath\omega_0)^q\} \\
\mathrm{Im}\{\Delta Y_{11}(\omega_0)(\jmath\omega_0)^q\} \\
\vdots \\
\mathrm{Im}\{\Delta Y_{mm}(\omega_r)(\jmath\omega_r)^q\} \\
\mathrm{Re}\{\Delta Y_{11}(\omega_0)(\jmath\omega_0)^q\} \\
\vdots \\
\mathrm{Re}\{\Delta Y_{mm}(\omega_r)(\jmath\omega_r)^q\} \\
\mathrm{Im}\{\Delta Y_{mm}(\omega_r)(\jmath\omega_r)^q\}
\end{bmatrix}
\tag{3.27}
$$

When this is found, the corresponding z_{aug} is represented by:

$$z_{\text{par,aug},i} = \frac{D(s) - D_{z,\text{par},i}(s)}{N_{\text{par},i}(s)} \tag{3.28}$$

for the parallel augmentation case. For the series case, the same procedure is followed to find the coefficients of $D_{z,\text{ser},k}(s) = d_{z,\text{ser},k,q}s^q + \cdots + d_{z,\text{ser},k,0}$. When they are found, the corresponding z_{aug} is given by:

$$z_{\text{ser,aug},k} = -\frac{N_{\text{ser},k}(s)}{D(s) - D_{z,\text{ser},k}(s)} \tag{3.29}$$

These rational functions are then passed through an order reduction algorithm. This removes the unneeded poles introduced by (3.18) and (3.19) as described above. One simple way to accomplish this is to convert the augmentations to a tabulated form based on the original sampling of ω and then fit it to a new function using a technique described in Section 5.3.

As mentioned before, the formulation of (3.8) does not account for the mutual effects among simultaneous augmentations. However, these effects tend to be relatively small. This is a valid assumption as the S-ECM response is expected to be reasonably close to the device's measured response and, in addition, these impedances are being added to refine the response (to reduce the error). An iterative method can be used to reduce the impact of this assumption. This is described later, in Section 5.2.

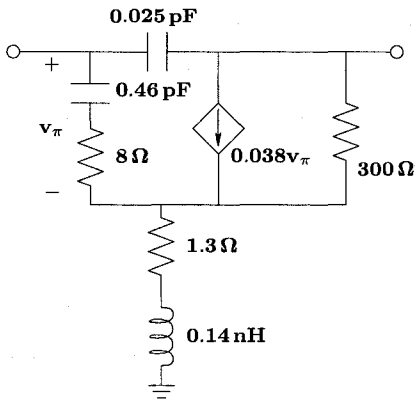

Figure 3.3: S-ECM for the FET Small-Signal Behaviour

3.5 Numerical Results

3.5.1 Small-Signal Transistor Model

The test case under consideration corresponds to the modelling of the small-signal behaviour of a field-effect transistor (FET). For the purpose of algorithm validation, the multi-port behaviour of the device is extracted using the full small-signal model described in [7]. The resulting data is treated as the measured data.

To begin with, the S-ECM shown in Figure 3.3 is considered to characterize this data. A sample comparison of the S-ECM behaviour with the measured data is given in Figures 3.4 to 3.11. The response of the S-ECM is the dotted line while the measured data is shown by the circle markers. As seen, the measured data and S-ECM match accurately at lower frequencies, however, deviate significantly at higher frequencies.

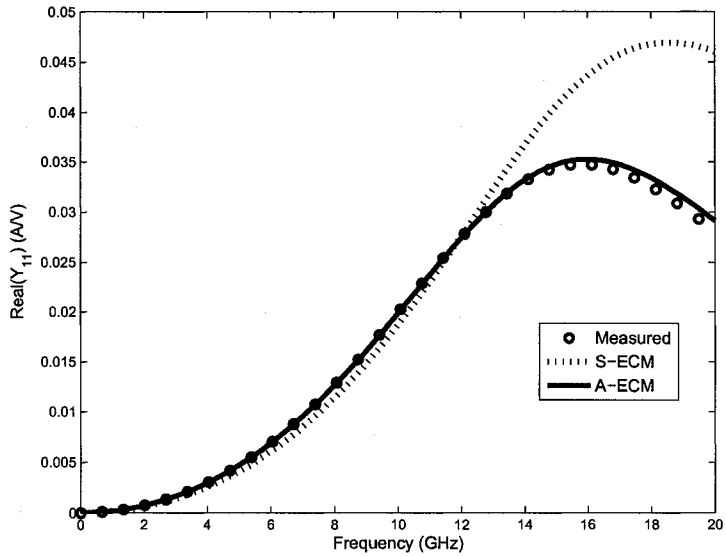

Figure 3.4: FET Model Accuracy Comparison (Real $Y_{11}(s)$)

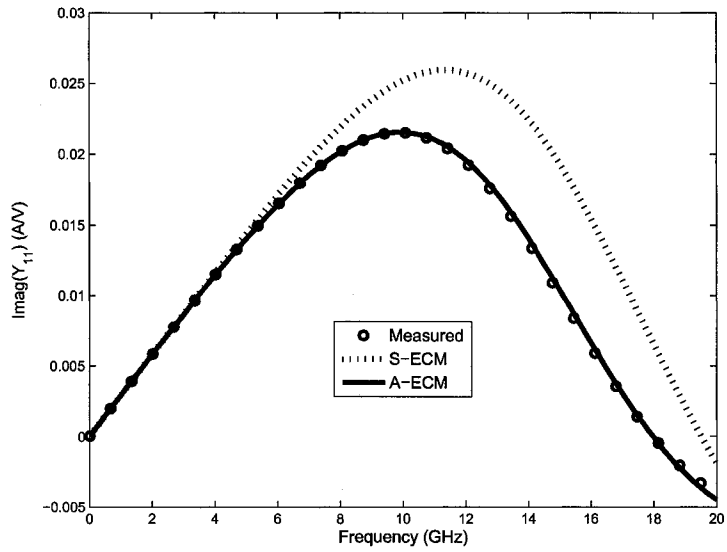

Figure 3.5: FET Model Accuracy Comparison (Imaginary $Y_{11}(s)$)

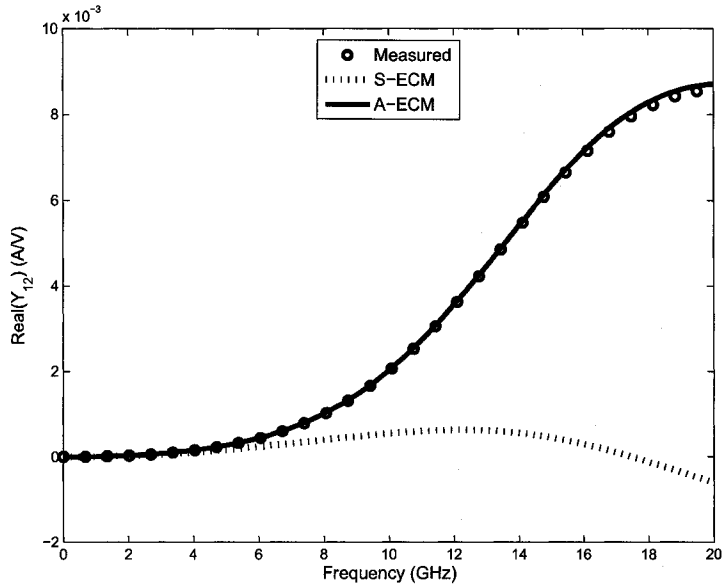

Figure 3.6: FET Model Accuracy Comparison (Real $Y_{12}(s)$)

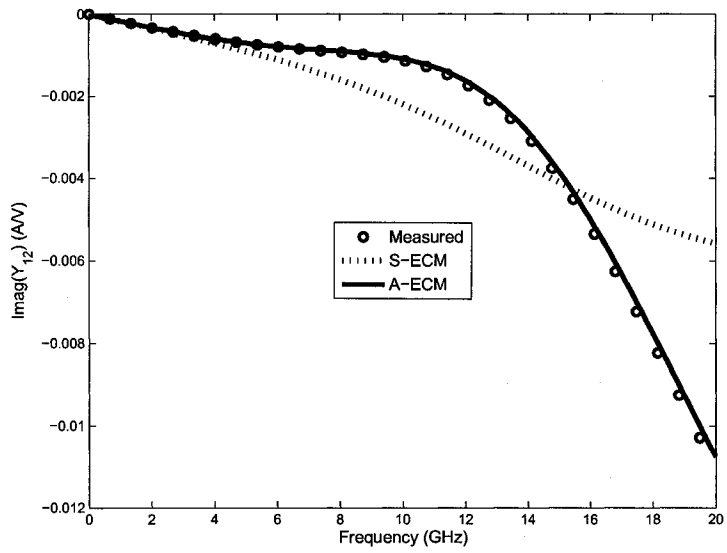

Figure 3.7: FET Model Accuracy Comparison (Imaginary $Y_{12}(s)$)

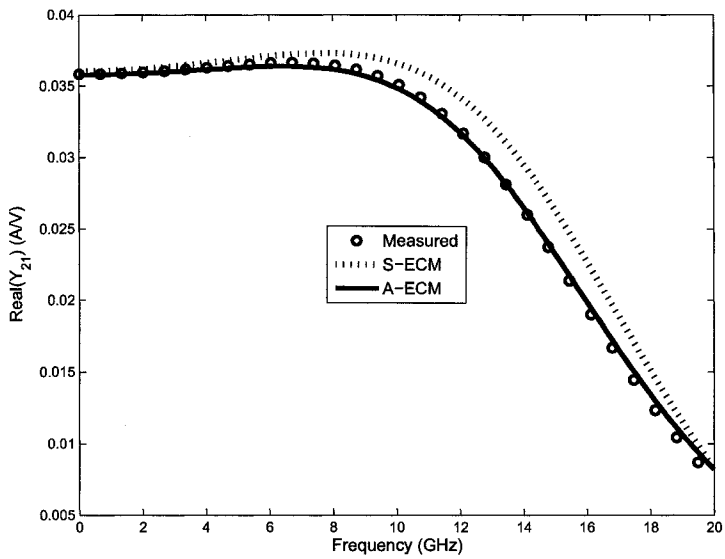

Figure 3.8: FET Model Accuracy Comparison (Real $Y_{21}(s)$)

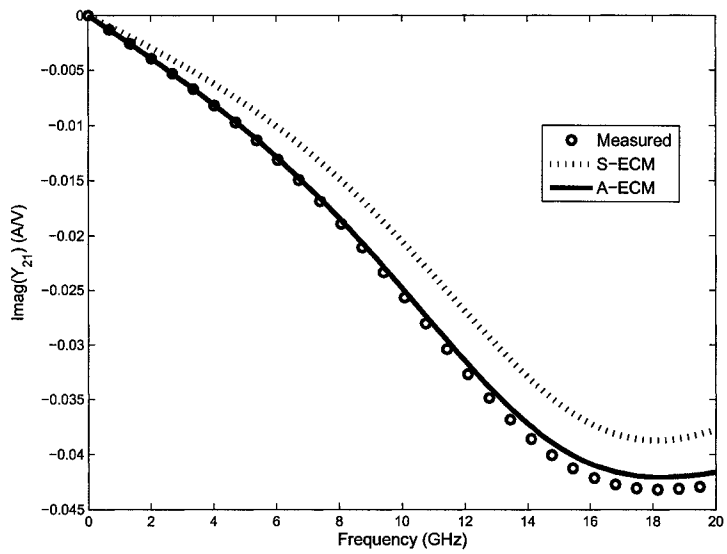

Figure 3.9: FET Model Accuracy Comparison (Imaginary $Y_{21}(s)$)

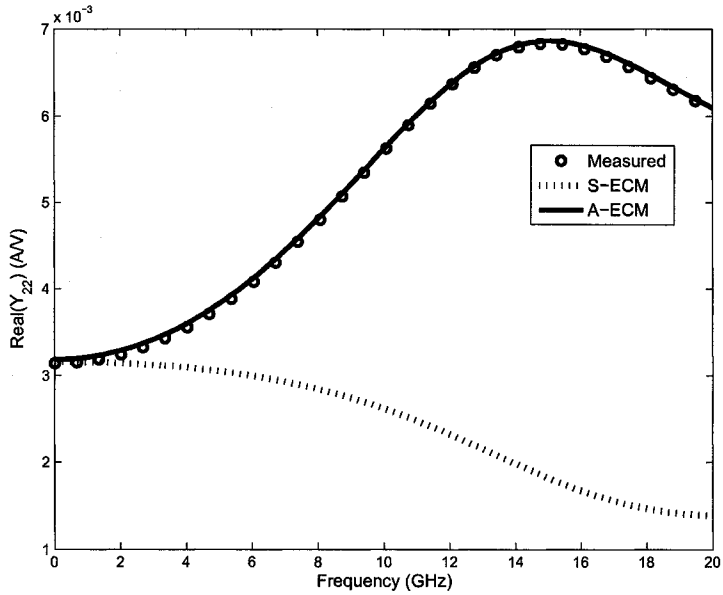

Figure 3.10: FET Model Accuracy Comparison (Real $Y_{22}(s)$)

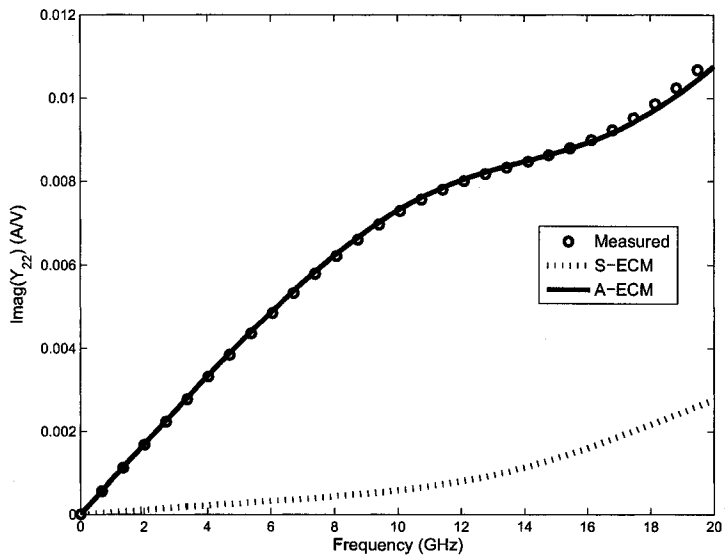

Figure 3.11: FET Model Accuracy Comparison (Imaginary $Y_{22}(s)$)

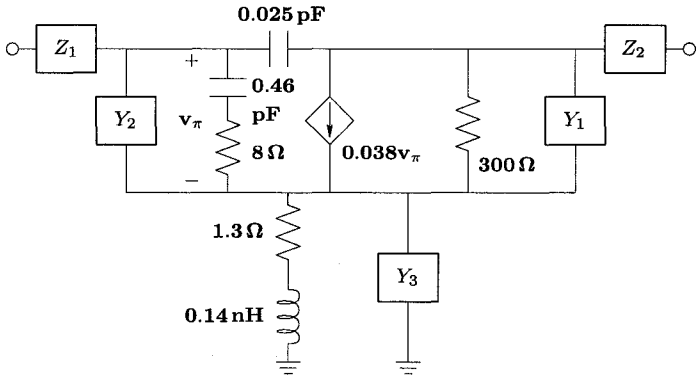

Figure 3.12: FET A-ECM Showing Location of Augmentations

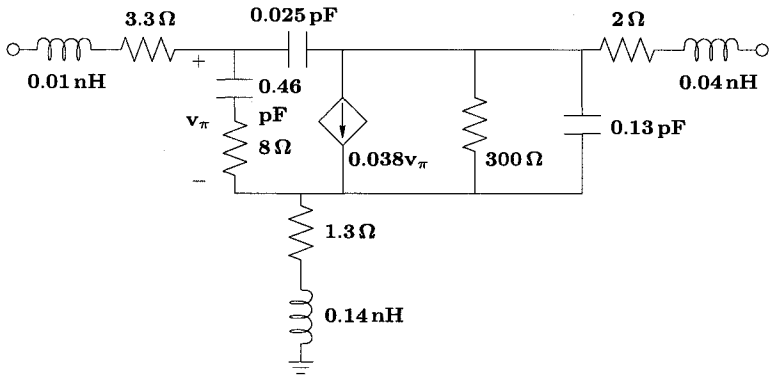

Figure 3.13: FET Final A-ECM

Next, the proposed algorithm was applied on the S-ECM to modify it so as to match its behaviour with the measured data over the entire frequency region. In the validation experiment, three parallel impedances, Y_1 through Y_3, and two series impedances, Z_1 and Z_2, were added to the S-ECM at various nodes as shown in Figure 3.12.

Subsequently, the proposed algorithm was applied to find values for each of the

impedances simultaneously. The rational functions used in the initial fitting were on the order of 11/11. For a good fit, the initial order has to be higher than what is necessary for the individual augmentations as discussed. It was found that Y_2 and Y_3 were open circuits. Following iterations and the augmentation order reduction, the order of each individual augmentation was 1/0 for Z_1 and Z_2 and 0/1 for Y_3.

With the order of the augmentations being so small, they were directly synthesized into the circuit elements shown in Figure 3.13. It is noted that the final values of these elements match the original model of [7] within a small margin attributable to numerical error.

A comparison of the response of the A-ECM with the measured data can also be found in Figures 3.4 to 3.8. The response of the A-ECM is shown as the solid line. As seen, they match accurately and the high frequency errors have been reduced in the A-ECM. In addition, the entire process of identifying the A-ECM required only 24 seconds (on a Sun Blade 1500) using the proposed algorithm.

3.5.2 Spiral Inductor

The second example is of a spiral inductor model. The measured characteristic of this inductor is taken from data in [24]. A simplified double-pi model was created and the data was fit to it. This model and the corresponding component values are shown in Figure 3.14.

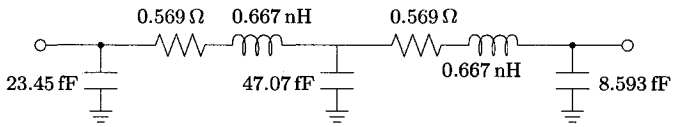

Figure 3.14: Simplified Inductor Model

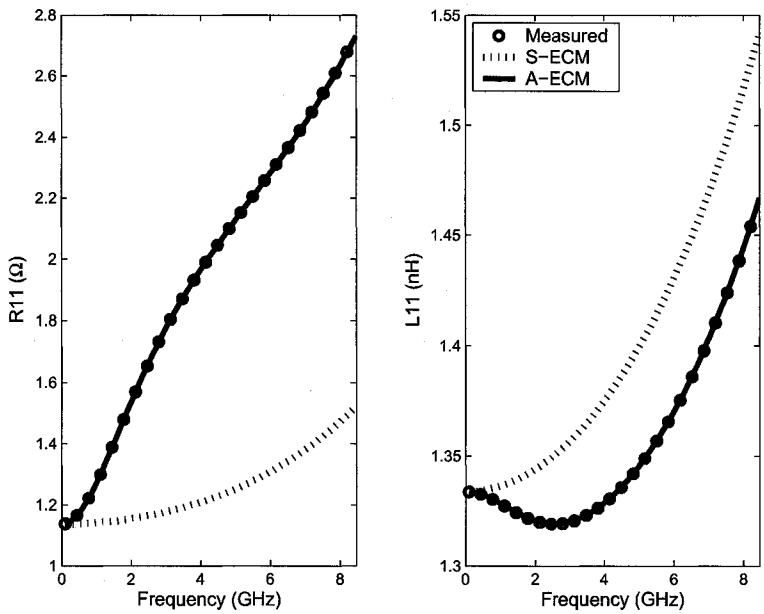

Figure 3.15: Inductor Models, Input Response

Figures 3.15 to 3.17 show the performance of this model compared to the measured values using the characteristics R_{11}, L_{11}, Q_{11}, R_{12} and L_{12} as defined in [24]. The circle markers are the actual measured responses while the dotted line is the response of the simplified model. Correlation is seen at the lower frequencies, however error increases greatly as the frequency increases.

To improve this model, it was decided to add two elements to the model using the

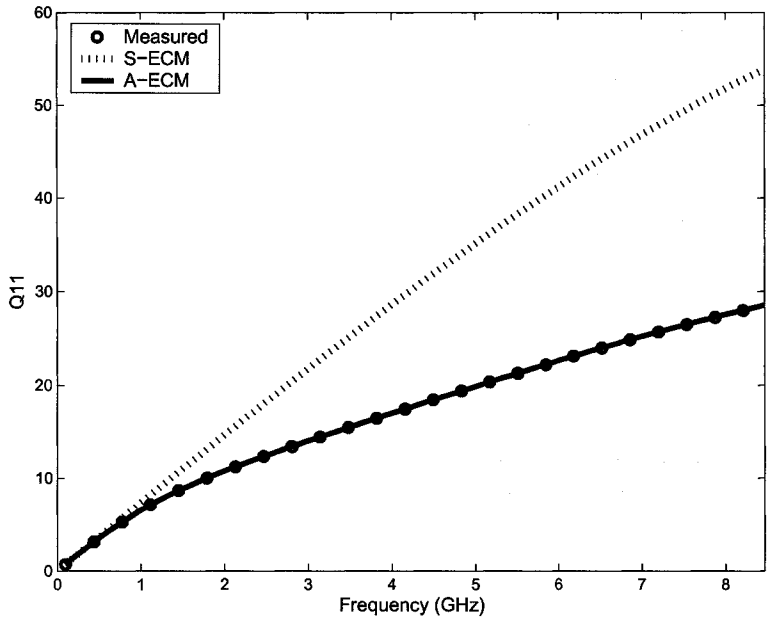

Figure 3.16: Inductor Models, Input Q-Factor

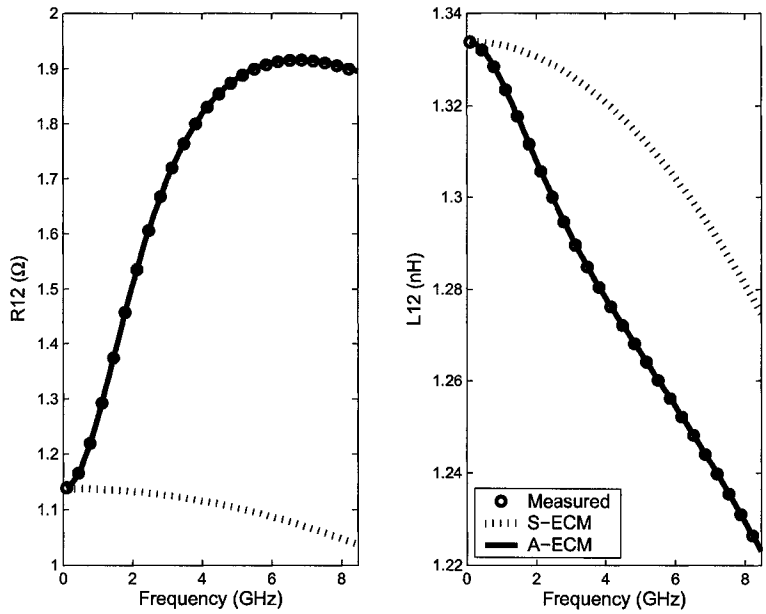

Figure 3.17: Inductor Models, Transmitted Response

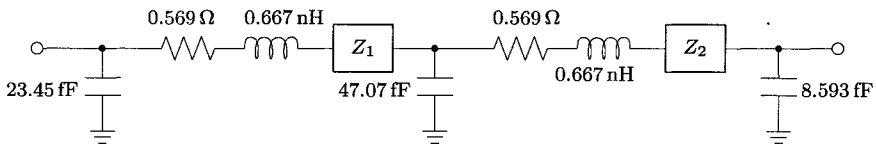

Figure 3.18: Inductor S-ECM Shown with Augmentation Locations

proposed algorithm. These are shown in Figure 3.18 and designated by Z_1 and Z_2.

The proposed algorithm was used to find a representation for each augmentation as a rational function of the order 11/11. These impedances were then fit individually with a vector fit using 2 poles for both Z_1 and Z_2. These results were then synthesized and inserted into the model, shown in Figure 3.19. The new responses are shown in Figures 3.15 to 3.17. Again, the circle markers represent the measured response while

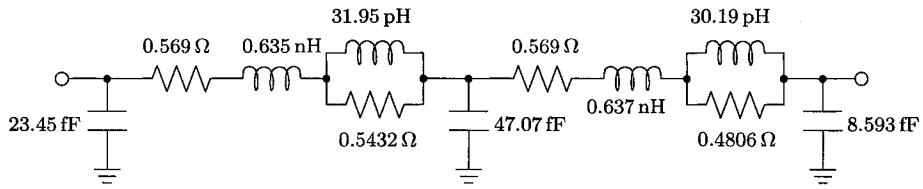

Figure 3.19: Final Inductor A-ECM

the solid line is the response of the augmented model. Adding these components has greatly reduced the error in the model for higher frequencies.

3.6 Summary

In this chapter, an algorithm was proposed to determine appropriate augmenting networks for a simple equivalent-circuit model (S-ECM) so as to better match the response of the physical device. The algorithm handles the cases where the augmentation is being connected across two existing nodes (parallel) or when it is being inserted into an existing branch (series). Through an approximation, the proposed algorithm was extended to the case of multiple simultaneous augmentations without reverting to a nonlinear optimization formulation. Finally, two examples from different areas were presented to demonstrate the effectiveness of this approach. In the next chapter, the algorithm will be further extended to handle the case of frequency-dependent transmission lines.

Chapter 4

Modelling Frequency-Dependent Transmission Line Parameters

4.1 Introduction

In the previous chapter, an algorithm was proposed to determine appropriate augmentations to add to a simple equivalent-circuit model (S-ECM) in order to improve its performance compared to measurements done on the actual device. In this chapter, the method is extended and applied to the specific case of frequency-dependent transmission lines. Frequency-domain models derived from frequency-domain parameters are usually not well suited for time-domain simulations. In the case of transmission lines, time-domain simulations are very important for signal integrity verification. To

provide a model suitable for time-domain simulations, the basic lumped transmission line model is improved with the algorithm developed in Chapter 3. This is covered in Section 4.2. In Section 4.3, the algorithm is extended to cover the case of multiple coupled lines. In each of these sections, numerical examples are presented to demonstrate the effectiveness of this approach.

4.2 Single Lines

Consider a single-conductor transmission line structure. Its characteristics are described by tabulated frequency-dependent per-unit-length RLCG parameters. These parameters are obtained from measurements, or by EM simulation. As discussed, frequency-dependent RLCG parameters are not suitable for time-domain simulations. For this reason, models containing linear elements are desirable.

A simple model of a transmission line is a lumped model with one section [25]. This model is illustrated in Figure 4.1. This model consists solely of standard circuit elements, and is therefore suitable for both frequency-domain and time-domain simulations. Additionally, the values of the elements map directly to the RLCG parameters. Unfortunately, the structure is too simple to handle frequency-dependent parameters.

However, this model does well at capturing the low-frequency characteristic of the transmission line. Therefore, the components are chosen to match the set of

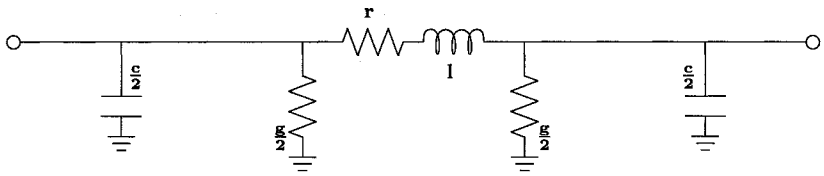

Figure 4.1: Basic Lumped Transmission Line Model

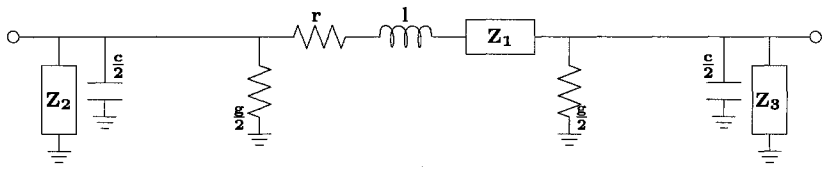

Figure 4.2: Augmented Lumped Transmission Line Model

frequency-dependent parameters for the lowest frequency point. To compensate for the frequency dependence of the various parameters, augmentations are added as shown in Figure 4.2. Z_1 is added to match the frequency dependence of R and L, while Z_2 and Z_3 are added for C and G.

To use the algorithm proposed in Chapter 3 to find appropriate networks for each augmentation, it is necessary to have a set of y-parameters derived from measurements. The measurements in this case are the RLCG parameters, so a means to convert these to y-parameters is needed. The telegrapher's equations [10] describe the transmission line's performance in terms of the RLCG parameters and are given

by

$$\frac{\partial}{\partial x}v(x,t) = -Ri(x,t) - L\frac{\partial}{\partial t}i(x,t) \tag{4.1}$$

$$\frac{\partial}{\partial x}i(x,t) = -Gv(x,t) - C\frac{\partial}{\partial t}v(x,t) \tag{4.2}$$

In the Laplace domain, these are rewritten as

$$\frac{\partial}{\partial x}V(x,s) = -(R+sL)I(x,s) \tag{4.3}$$

$$\frac{\partial}{\partial x}I(x,s) = -(G+sC)V(x,s) \tag{4.4}$$

In matrix form, these become

$$\frac{\partial}{\partial x}\begin{bmatrix} V(x,s) \\ I(x,s) \end{bmatrix} = (\boldsymbol{D}+s\boldsymbol{E})\begin{bmatrix} V(x,s) \\ I(x,s) \end{bmatrix} \tag{4.5}$$

where

$$\boldsymbol{D} = \begin{bmatrix} 0 & -R \\ -G & 0 \end{bmatrix} \tag{4.6}$$

$$\boldsymbol{E} = \begin{bmatrix} 0 & -L \\ -C & 0 \end{bmatrix} \tag{4.7}$$

If the transmission line is connected as the two-port network in Figure 4.3 and is of length d, the above differential equation can be solved if the terminal condition of port 1 is imposed. Using standard differential equation techniques, the solution of (4.5) becomes

$$\begin{bmatrix} V(d,s) \\ I(d,s) \end{bmatrix} = \mathrm{e}^{(\boldsymbol{D}+s\boldsymbol{E})d}\begin{bmatrix} V(0,s) \\ I(0,s) \end{bmatrix} \tag{4.8}$$

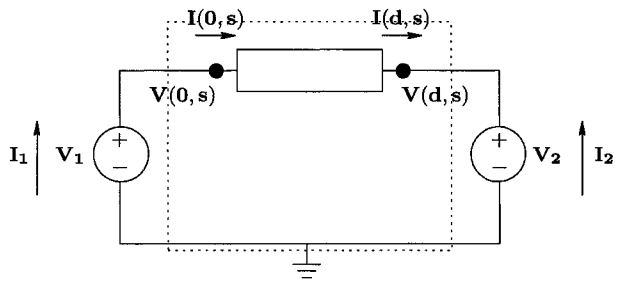

Figure 4.3: Single Transmission Line as a Two-Port Network

where $e^{\boldsymbol{A}}$ is the matrix exponential of $\boldsymbol{A}$. The matrix exponential is defined for a matrix $\boldsymbol{A} \in \mathbb{C}^{n\times n}$ as $e^{\boldsymbol{A}} = \boldsymbol{P}^{-1}\text{diag}\{e^{\lambda_1}, \cdots, e^{\lambda_n}\}\boldsymbol{P}$ where $\boldsymbol{P}$ is the matrix of Eigenvectors of $\boldsymbol{A}$ and $\{\lambda_1, \cdots, \lambda_n\}$ are the corresponding Eigenvalues such that $\boldsymbol{A} = \boldsymbol{P}^{-1}\text{diag}\{\lambda_1, \cdots, \lambda_n\}\boldsymbol{P}$.

The transmission network parameters, $\boldsymbol{T}$, the inverse of the ABCD parameters, are defined as:

$$\begin{bmatrix} V_2 \\ -I_2 \end{bmatrix} = \boldsymbol{T} \begin{bmatrix} V_1 \\ I_1 \end{bmatrix} \tag{4.9}$$

Comparing (4.8) and (4.9) with the notation shown in Figure 4.3, it is clear that

$$\boldsymbol{T} = \begin{bmatrix} t_{11} & t_{12} \\ t_{21} & t_{22} \end{bmatrix} = e^{(\boldsymbol{D}+s\boldsymbol{E})d} \tag{4.10}$$

These parameters can be converted to y-parameters with the following relation [10]

$$\boldsymbol{Y} = \begin{bmatrix} -\frac{t_{11}}{t_{12}} & \frac{1}{t_{12}} \\ -t_{21} + \frac{t_{22}t_{11}}{t_{12}} & -\frac{t_{22}}{t_{12}} \end{bmatrix} \tag{4.11}$$

With this relation, y-parameters can be obtained from the RLCG parameters for each frequency point. At this point, the problem can be solved using the method described in Chapter 3. This method provides a more generalized and simple method to model frequency-dependent losses in transmission lines than traditional approaches such as those outlined in [25]. To demonstrate the effectiveness of this procedure, an example is presented.

4.2.1 Numerical Results

Cable Model

A lossy single-conductor cable was chosen as an example of a transmission line with frequency-dependent parameters. The 'measured' data was taken from the Line 4 example presented in [26]. The S-ECM for this cable, as described previously, is shown in Figure 4.4. The component values were set to match the low-frequency characteristics. To model the high-frequency characteristic of the cable, the proposed augmentations were added to the series branch and to each shunt. The algorithm found that the shunt augmentations were not needed, so these were excluded. Optimal values for the remaining augmentation were found with a rational function of order 6/5. The higher order was needed to best match the rapid change in inductance at lower frequencies. As this rational function is passive and represents a single port network, the technique described in Section 2.4 was used to synthesize it into a ladder

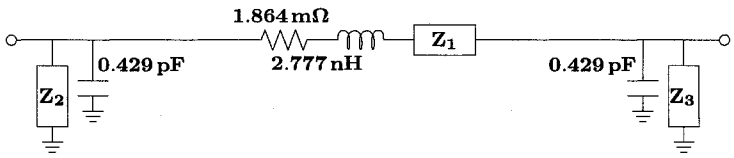

Figure 4.4: Cable S-ECM shown with location of augmentations

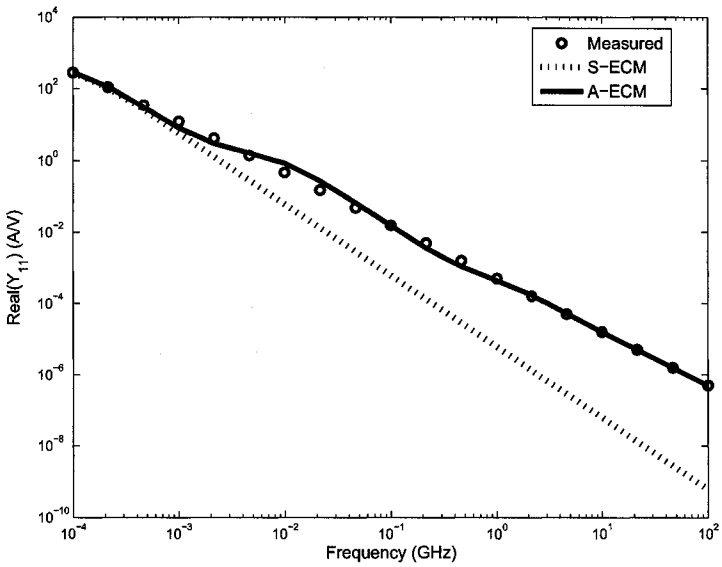

Figure 4.5: Real Part of Y_{11} for the Cable Models

network. This network was inserted into the simple model, and the final model is shown in Figure 4.9.

Results are shown in Figures 4.5 to 4.8. The circle markers show the measured data, the dotted line corresponds to the S-ECM before augmenting, and the solid line corresponds to the final A-ECM. As is clearly seen, the augmentations bring the response of the ECM much closer to that of the measurements. The entire process of

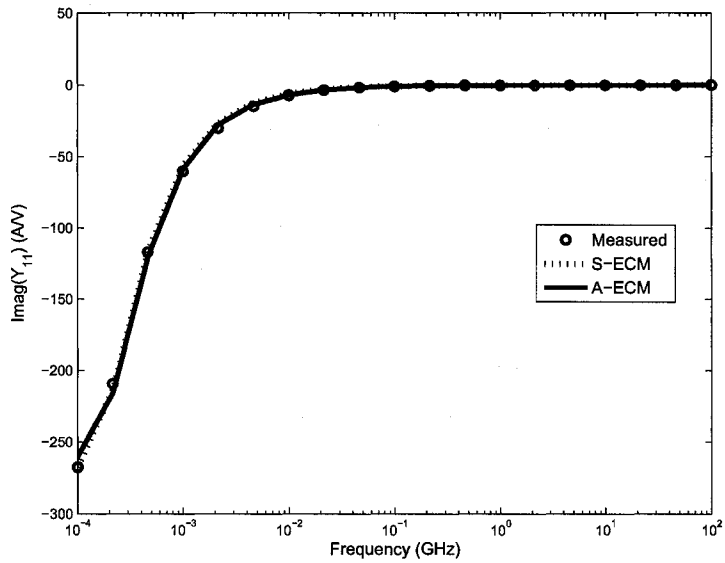

Figure 4.6: Imaginary Part of Y_{11} for the Cable Models

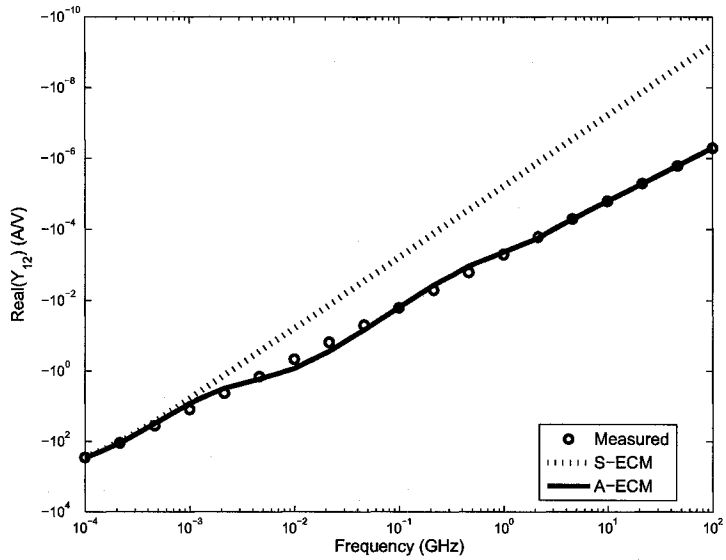

Figure 4.7: Real Part of Y_{12} for the Cable Models

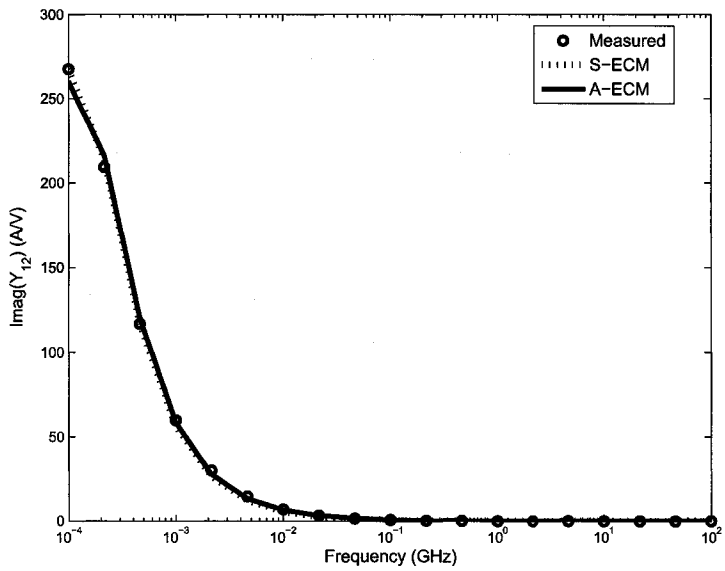

Figure 4.8: Imaginary Part of Y_{12} for the Cable Models

identifying the A-ECM required only 12 seconds (on a Sun Blade 1500).

4.3 Coupled Lines

In this section, the technique of Section 4.2 is extended to the more general case of a multi-conductor transmission line. Consider an m-conductor transmission line system. For the purpose of illustration, the case where $m = 2$ is considered (without the loss of generality). To model each line, the standard pi-model is matched to the RLCG parameters of each line as shown in Figure 4.10.

Once again, this simple model cannot capture the frequency dependence of the RLCG parameters. It also requires modification to handle coupling between the lines.

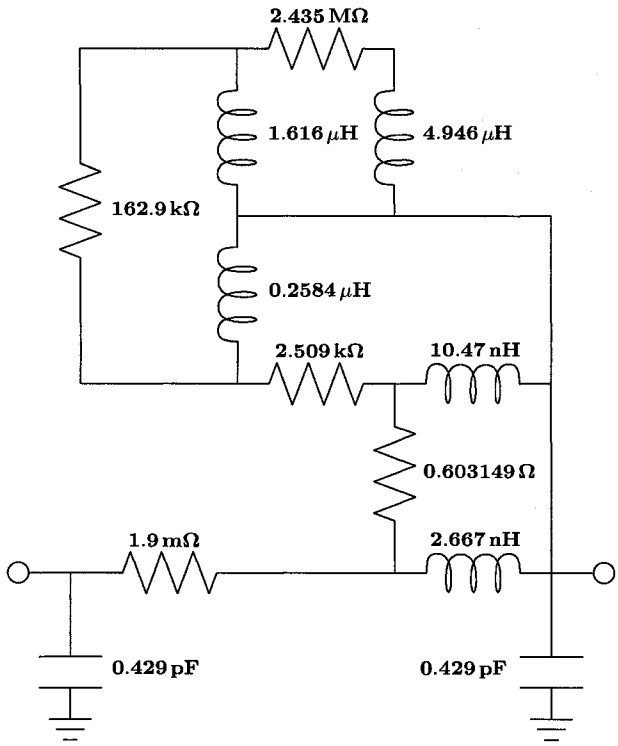

Figure 4.9: Cable S-ECM shown with synthesized augmentation

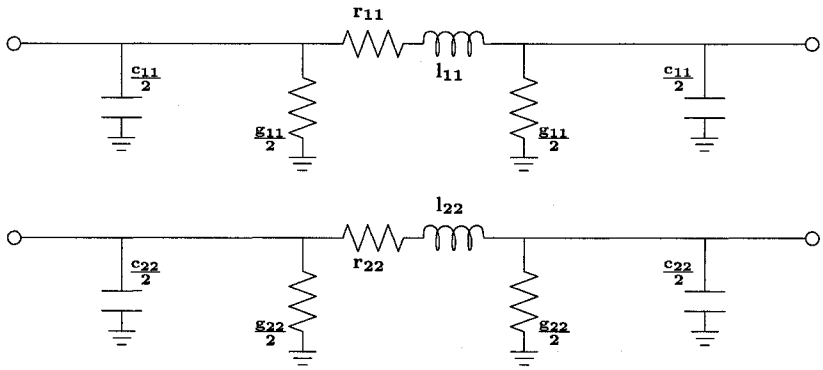

Figure 4.10: Original S-ECM of the Two-Conductor Transmission Line

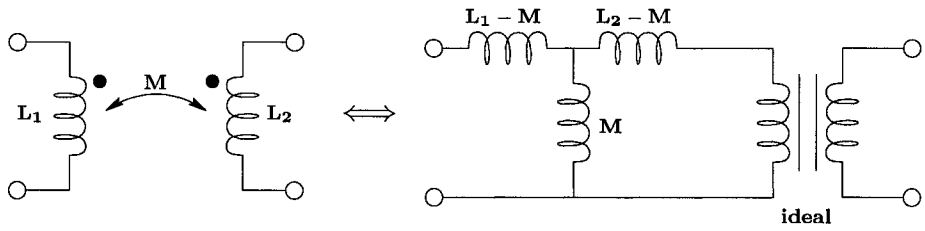

Figure 4.11: Transformation for Augmenting Mutual Inductance

To include coupling, mutual inductance and mutual capacitance are generally inserted between the lines. Usually, mutual inductances can only be characterized by two-port networks due to their nature. In the proposed algorithm, instead of directly adding the mutual inductance, the transformation given in Figure 4.11 will be used. This allows the mutual inductance to be treated as a set of standard inductor elements.

To capture the frequency dependence of the RLCG parameters, various subnetworks are added into the pi-model. These subnetworks can be of any needed complexity, but must be able to be represented as the driving-point impedance of a single port network. This version of the model is shown in Figure 4.12. The goal of each added subnetwork is the following:

- Z_1 captures the L_{12} parameter and its frequency dependence.
- Z_2 captures the frequency dependence of R_{11} and L_{11} and compensates for the mutual inductance L_{12} as required by the transformation of Figure 4.11.
- Z_3 does the same for R_{22} and L_{22}.

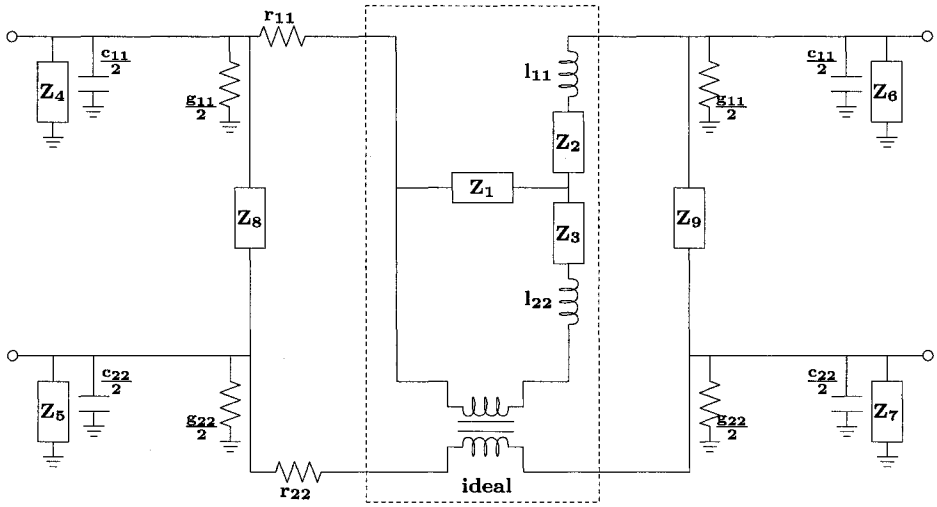

Figure 4.12: Transformed Model shown with Augmentation Locations

- Z_4 and Z_6 add the frequency dependence of C_{11} and G_{11} to the model.
- Z_5 and Z_7 do the same for C_{22} and G_{22}.
- Z_8 and Z_9 model the C_{12} and G_{12} parameters.

When extending this technique to the general case of m coupled lines, the L_{ii} element for the i^{th} line is split into $(m-1)$ equal sections. This inductor and a corresponding inductor in the j^{th} line are replaced with the transformation in Figure 4.11 to capture the mutual inductance given by L_{ij}.

As with the single conductor case, it is desired to use the algorithm proposed in Chapter 3 to find appropriate networks for each augmentation. A set of y-parameters derived from measurements are therefore required. The process given in Section 4.2

is followed to convert the matrix RLCG parameters for m coupled lines to a set of y-parameters for a $2m$-port network. The telegrapher's equations for coupled transmission lines [10] are given as

$$\frac{\partial}{\partial x}\boldsymbol{v}(x,t) = -\boldsymbol{R}\boldsymbol{i}(x,t) - \boldsymbol{L}\frac{\partial}{\partial t}\boldsymbol{i}(x,t) \tag{4.12}$$

$$\frac{\partial}{\partial x}\boldsymbol{i}(x,t) = -\boldsymbol{G}\boldsymbol{v}(x,t) - \boldsymbol{C}\frac{\partial}{\partial t}\boldsymbol{v}(x,t) \tag{4.13}$$

For a system with m coupled lines, $\boldsymbol{v}(x,t) = [v_1(x,t) \quad \cdots \quad v_m(x,t)]^{\mathrm{t}}$ and $\boldsymbol{i}(x,t) = [i_1(x,t) \quad \cdots \quad i_m(x,t)]^{\mathrm{t}}$ where $v_j(x,t)$ is the voltage and $i_j(x,t)$ is the current on the j^{th} line at position x at time t.

In the Laplace domain, these are rewritten as

$$\frac{\partial}{\partial x}\boldsymbol{V}(x,s) = -(\boldsymbol{R}+s\boldsymbol{L})\boldsymbol{I}(x,s) \tag{4.14}$$

$$\frac{\partial}{\partial x}\boldsymbol{I}(x,s) = -(\boldsymbol{G}+s\boldsymbol{C})\boldsymbol{V}(x,s) \tag{4.15}$$

In matrix form, these become

$$\frac{\partial}{\partial x}\begin{bmatrix}\boldsymbol{V}(x,s)\\ \boldsymbol{I}(x,s)\end{bmatrix} = (\boldsymbol{D}+s\boldsymbol{E})\begin{bmatrix}\boldsymbol{V}(x,s)\\ \boldsymbol{I}(x,s)\end{bmatrix} \tag{4.16}$$

where

$$\boldsymbol{D} = \begin{bmatrix}\boldsymbol{0}_{m\times m} & -\boldsymbol{R}\\ -\boldsymbol{G} & \boldsymbol{0}_{m\times m}\end{bmatrix} \tag{4.17}$$

$$\boldsymbol{E} = \begin{bmatrix}\boldsymbol{0}_{m\times m} & -\boldsymbol{L}\\ -\boldsymbol{C} & \boldsymbol{0}_{m\times m}\end{bmatrix} \tag{4.18}$$

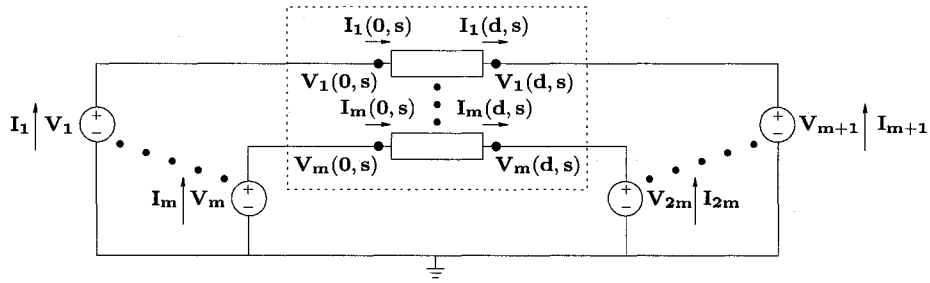

Figure 4.13: Coupled Transmission Lines as a Multi-Port Network

If the transmission line is connected as the multi-port network in Figure 4.13 and is of length d, the above differential equation can be solved if the terminal condition of ports 1 through m are imposed. Using standard differential equation techniques, the solution of (4.16) becomes

$$\begin{bmatrix} \boldsymbol{V}(d,s) \\ \boldsymbol{I}(d,s) \end{bmatrix} = \mathrm{e}^{(\boldsymbol{D}+s\boldsymbol{E})d} \begin{bmatrix} \boldsymbol{V}(0,s) \\ \boldsymbol{I}(0,s) \end{bmatrix} \tag{4.19}$$

The transmission network parameters, $\boldsymbol{T}$, the inverse of the ABCD parameters, are defined as:

$$\begin{bmatrix} V_{m+1} \\ \vdots \\ V_{2m} \\ -I_{m+1} \\ \vdots \\ -I_{2m} \end{bmatrix} = \boldsymbol{T} \begin{bmatrix} V_1 \\ \vdots \\ V_m \\ I_1 \\ \vdots \\ I_m \end{bmatrix} \tag{4.20}$$

Comparing (4.19) and (4.20) with the notation shown in Figure 4.13, it is clear that

$$\boldsymbol{T} = \begin{bmatrix} \boldsymbol{T}_{11} & \boldsymbol{T}_{12} \\ \boldsymbol{T}_{21} & \boldsymbol{T}_{22} \end{bmatrix} = \mathrm{e}^{(\boldsymbol{D}+s\boldsymbol{E})d} \tag{4.21}$$

where $\boldsymbol{T}_{11} \cdots \boldsymbol{T}_{22}$ are each in $\mathfrak{C}^{m\times m}$.

These parameters can be converted to y-parameters with the following relation [10]

$$\boldsymbol{Y} = \begin{bmatrix} -\boldsymbol{T}_{12}^{-1}\boldsymbol{T}_{11} & \boldsymbol{T}_{12}^{-1} \\ -\boldsymbol{T}_{21} + \boldsymbol{T}_{22}\boldsymbol{T}_{12}^{-1}\boldsymbol{T}_{11} & -\boldsymbol{T}_{22}\boldsymbol{T}_{12}^{-1} \end{bmatrix} \tag{4.22}$$

With this relation, y-parameters can be obtained from the RLCG parameters for each frequency point. At this point, the problem can be solved using the method described in Chapter 3. Next, an example is presented to demonstrate the effectiveness of the proposed algorithm.

4.3.1 Numerical Results

Coupled Line Model

In this example, the validity and efficiency of the proposed algorithm are demonstrated. The 'measured' data was taken from the Line 2 example presented in [26]. The measured RLCG matrix parameters were converted to the corresponding y-parameters for a unit length. The lumped ECM of Figure 4.12 was selected to represent these lines. The component values were chosen to match the low-frequency

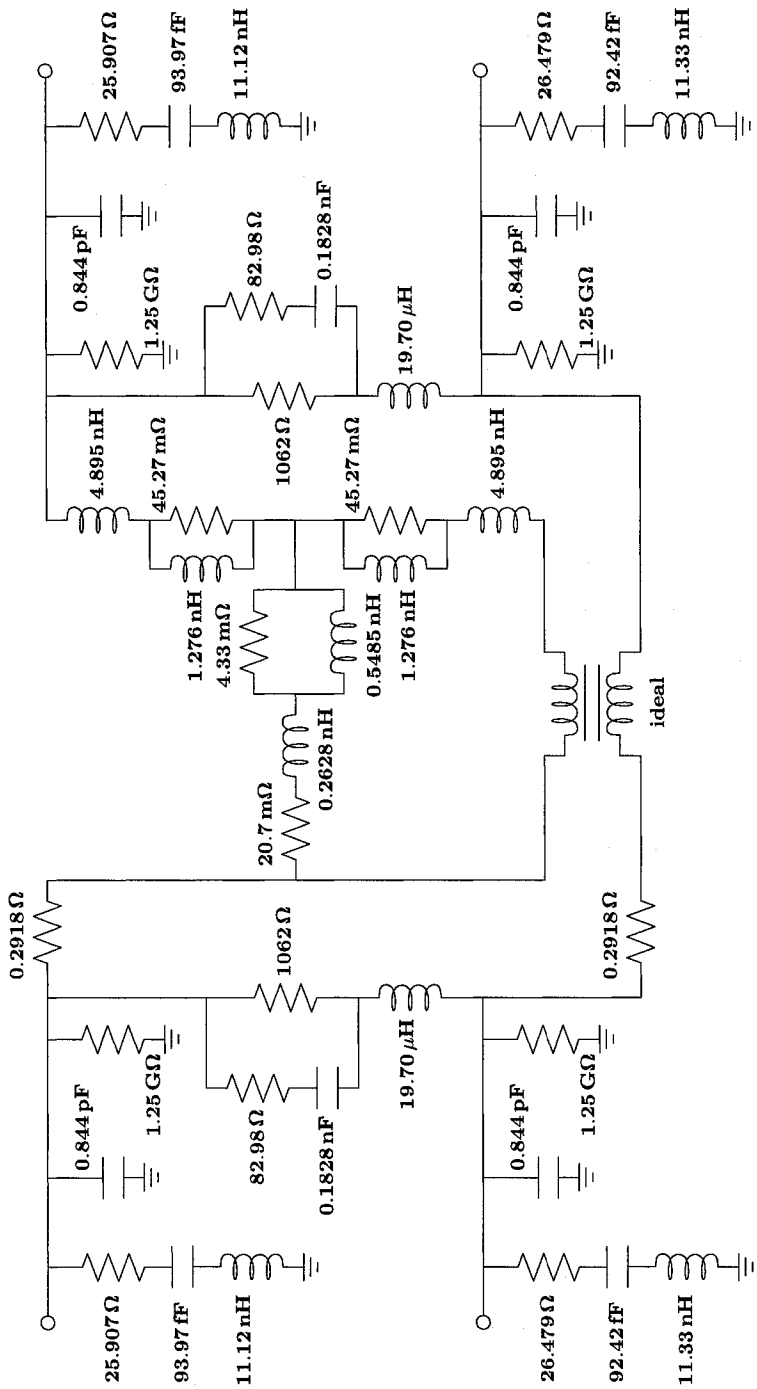

Figure 4.14: Final A-ECM for the Coupled Line Example

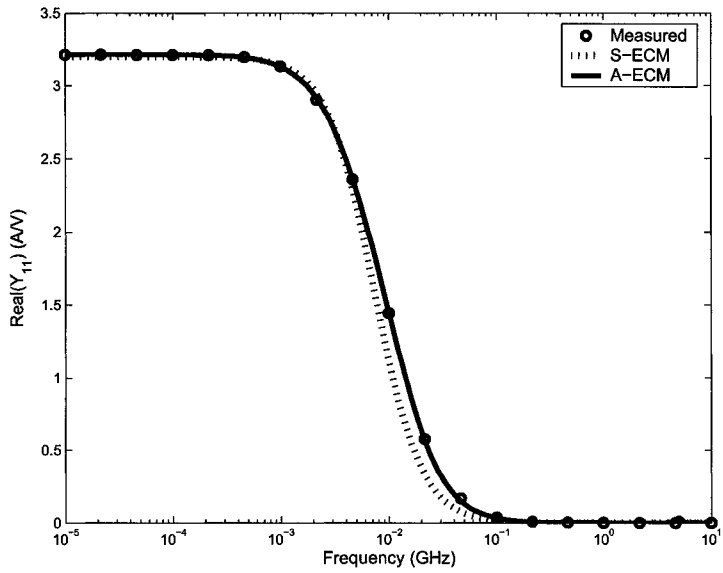

Figure 4.15: Model and Measured Real Y_{11} for Coupled Transmission Line

characteristics.

Next, the proposed algorithm was applied on the ECM to modify it so as to match its behaviour with the measured data over the entire frequency region. The resulting augmentations were fit to a rational function using vector fit with between 1 and 2 poles. Passivity was enforced for these rational functions and they were synthesized into RLC networks. When they were placed in the model, the final A-ECM in Figure 4.14 was obtained.

A comparison of the response of the final ECM with the measured data can also be found in Figures 4.15 to 4.22. The circle markers show the measured data, the dotted line corresponds to the S-ECM before augmenting, and the solid line corresponds to

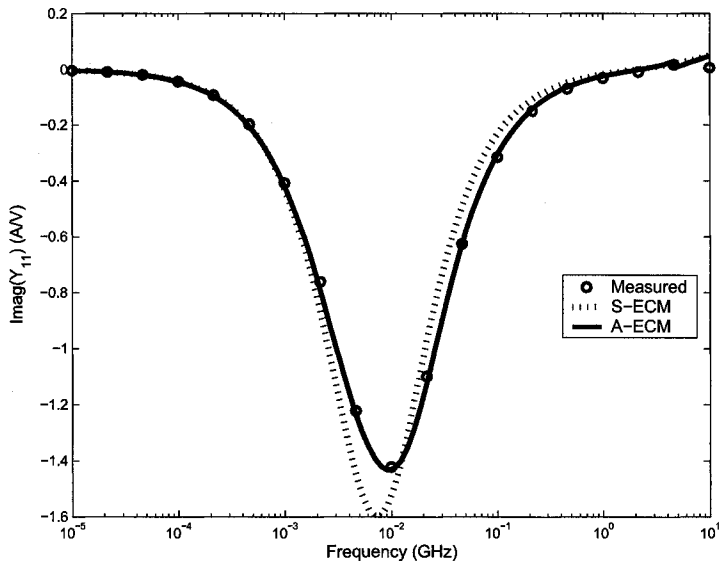

Figure 4.16: Model and Measured Imaginary Y_{11} for Coupled Transmission Line

the final A-ECM. As seen, they match accurately and the errors have been corrected in the improved A-ECM. The entire process of identifying the final ECM required only 27 seconds (on a Sun Blade 1500) using the proposed algorithm.

4.4 Summary

In this chapter, the proposed algorithm was extended to the case of frequency-dependent transmission lines. This allows an accurate model to be derived that can be used for both frequency-domain and time-domain simulations. With the application of an equivalent circuit for mutual inductance, the algorithm was also applied to the case of multiple coupled lines. An example was presented for each case to demon-

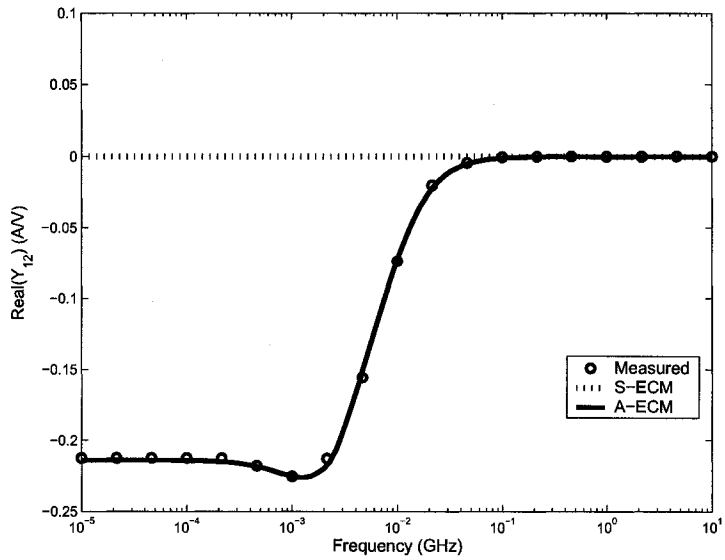

Figure 4.17: Model and Measured Real Y_{12} for Coupled Transmission Line

strate the effectiveness of this approach. In the next chapter, various implementation issues will be discussed with solutions presented.

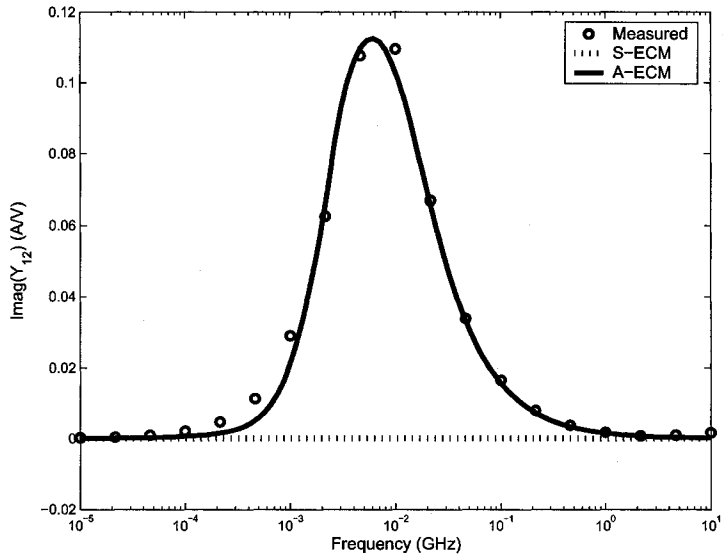

Figure 4.18: Model and Measured Imaginary Y_{12} for Coupled Transmission Line

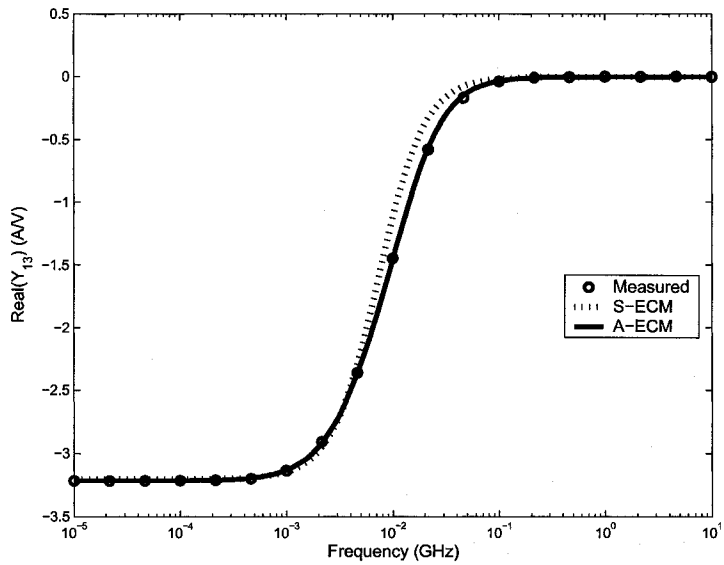

Figure 4.19: Model and Measured Real Y_{13} for Coupled Transmission Line

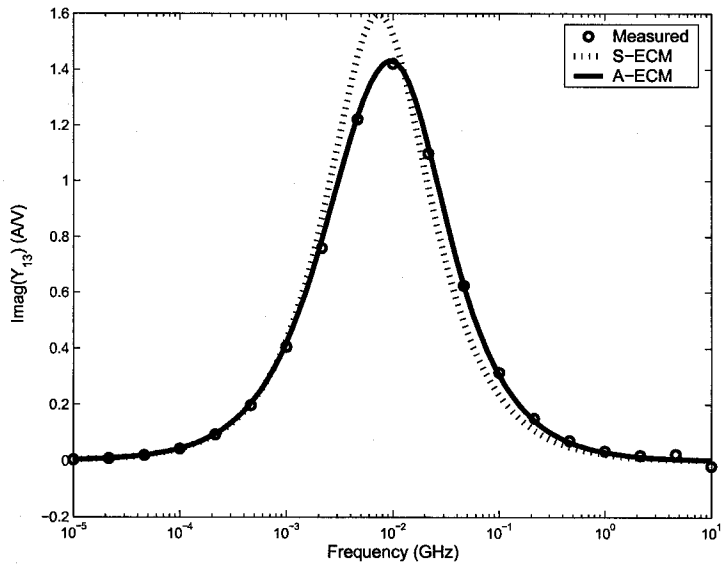

Figure 4.20: Model and Measured Imaginary Y_{13} for Coupled Transmission Line

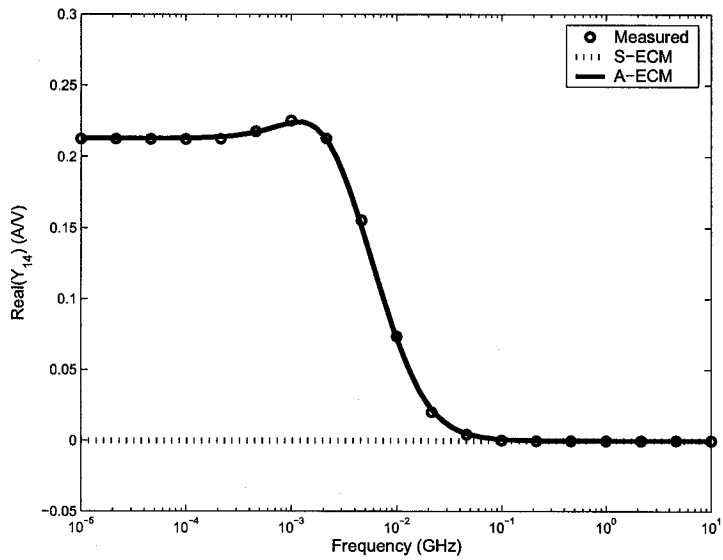

Figure 4.21: Model and Measured Real Y_{14} for Coupled Transmission Line

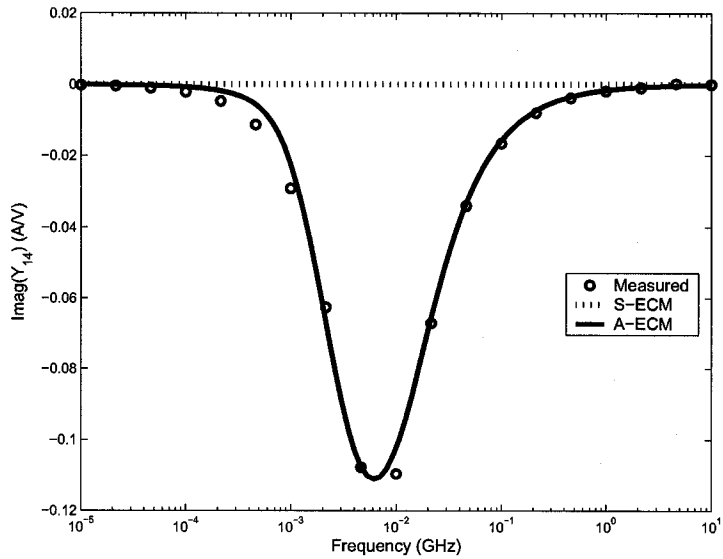

Figure 4.22: Model and Measured Imaginary Y_{14} for Coupled Transmission Line

Chapter 5

Implementation Issues

5.1 Introduction

In this chapter, various implementation issues concerning the algorithm developed in Chapters 3 and 4 will be discussed. The first issue, in Section 5.2, discusses the error introduced by the approximation made in Section 3.4 to handle multiple augmentations. In this case that this error is not negligible, an alternative implementation is discussed. Next, in Section 5.3, various options for implementing the rational function fitting procedure are discussed. When using these algorithms on models that must be accurate over a wide bandwidth, the large difference between the maximum and minimum frequency can introduce numerical errors. To overcome this difficulty, solutions are presented in Sections 5.4 and 5.5.

5.2 Refinement Iterations

In Section 3.4, an algorithm was proposed to find appropriate networks for multiple augmentations simultaneously. As discussed there, this was possible by assuming the effect of each augmentation was independent of the others. In many cases, the error introduced by this approximation is negligible, but in others it is desirable to remove this error.

To begin, first the source of this error will be described. In the derivation by Rohrer presented in Section 2.3.2, the effect can be seen intuitively by applying the notation of (2.54) to (2.55)

$$\Delta \boldsymbol{x} = \frac{-v_{\text{oc}}}{z_{\text{aug,par}} + z_{\text{th}}} \boldsymbol{A}^{-1} \boldsymbol{\xi} \tag{5.1}$$

where $\Delta \boldsymbol{x}$ is the effect on the MNA variables of adding a single parallel augmentation $z_{\text{aug,par}}$. If this is extended to the case where two augmentations are added, and assuming they are independent as is done with the approximation, the following is the overall effect

$$\Delta \boldsymbol{x} = \frac{-v_{\text{oc},1}}{z_{\text{aug,par},1} + z_{\text{th},1}} \boldsymbol{A}^{-1} \boldsymbol{\xi}_1 + \frac{-v_{\text{oc},2}}{z_{\text{aug,par},2} + z_{\text{th},2}} \boldsymbol{A}^{-1} \boldsymbol{\xi}_2 \tag{5.2}$$

It is clear that after the first augmentation is added, this would have had an effect on the open-circuit voltage ($v_{\text{oc},2}$), the Thévenin equivalent impedance ($z_{\text{th},2}$) and also the overall MNA matrix ($\boldsymbol{A}$) seen by the second augmentation. The magnitude of

these changes will depend on the configuration of the circuit and the location of the first augmentation relative to the second one.

To see the effect from a mathematical perspective, the derivation based on the Sherman-Morrison formula in Section 2.3.2 is considered. When two augmentations are added to a model, the modified MNA matrix will be

$$\hat{\boldsymbol{A}} = \boldsymbol{A} + \boldsymbol{\xi}_1 \boldsymbol{\xi}_1^{\mathrm{t}} z_{\mathrm{aug,par},1}^{-1} + \boldsymbol{\xi}_2 \boldsymbol{\xi}_2^{\mathrm{t}} z_{\mathrm{aug,par},2}^{-1} \tag{5.3}$$

The effect of adding the first impedance on the MNA matrix inverse, $\Delta(\boldsymbol{A}^{-1})_1$ is, from (2.67),

$$\Delta(\boldsymbol{A}^{-1})_1 = (\boldsymbol{A} + z_{\mathrm{aug,par},1}^{-1} \boldsymbol{\xi}_1 \boldsymbol{\xi}_1^{\mathrm{t}})^{-1} - \boldsymbol{A}^{-1} = \frac{\boldsymbol{A}^{-1} \boldsymbol{\xi}_1 \boldsymbol{\xi}_1^{\mathrm{t}} \boldsymbol{A}^{-1}}{-z_{\mathrm{aug,par},1} - \boldsymbol{\xi}_1^{\mathrm{t}} \boldsymbol{A}^{-1} \boldsymbol{\xi}_1} \tag{5.4}$$

Using the assumption that the first augmentation will not alter the effect of the second, the approximate effect of the second augmentation on the MNA matrix inverse, $\Delta(\tilde{\boldsymbol{A}}^{-1})_2$, is given by

$$\Delta(\tilde{\boldsymbol{A}}^{-1})_2 = (\boldsymbol{A} + z_{\mathrm{aug,par},2}^{-1} \boldsymbol{\xi}_2 \boldsymbol{\xi}_2^{\mathrm{t}})^{-1} - \boldsymbol{A}^{-1} = \frac{\boldsymbol{A}^{-1} \boldsymbol{\xi}_2 \boldsymbol{\xi}_2^{\mathrm{t}} \boldsymbol{A}^{-1}}{-z_{\mathrm{aug,par},2} - \boldsymbol{\xi}_2^{\mathrm{t}} \boldsymbol{A}^{-1} \boldsymbol{\xi}_2} \tag{5.5}$$

On the other hand, if it is considered that the first augmentation has already been added, applying (2.62) to find the actual effect of the second augmentation on the MNA matrix inverse, $\Delta(\boldsymbol{A}^{-1})_2$, results in

$$\Delta(\boldsymbol{A}^{-1})_2 = \left[(\boldsymbol{A} + z_{\mathrm{aug,par},1}^{-1} \boldsymbol{\xi}_1 \boldsymbol{\xi}_1^{\mathrm{t}}) + z_{\mathrm{aug,par},2}^{-1} \boldsymbol{\xi}_2 \boldsymbol{\xi}_2^{\mathrm{t}}\right]^{-1} - (\boldsymbol{A} + z_{\mathrm{aug,par},1}^{-1} \boldsymbol{\xi}_1 \boldsymbol{\xi}_1^{\mathrm{t}})^{-1} = \frac{(\boldsymbol{A} + z_{\mathrm{aug,par},1}^{-1} \boldsymbol{\xi}_1 \boldsymbol{\xi}_1^{\mathrm{t}})^{-1} \boldsymbol{\xi}_2 \boldsymbol{\xi}_2^{\mathrm{t}} (\boldsymbol{A} + z_{\mathrm{aug,par},1}^{-1} \boldsymbol{\xi}_1 \boldsymbol{\xi}_1^{\mathrm{t}})^{-1}}{-z_{\mathrm{aug,par},2} - \boldsymbol{\xi}_2^{\mathrm{t}} (\boldsymbol{A} + z_{\mathrm{aug,par},1}^{-1} \boldsymbol{\xi}_1 \boldsymbol{\xi}_1^{\mathrm{t}})^{-1} \boldsymbol{\xi}_2} \tag{5.6}$$

Therefore, it is seen that the source of the error is in the assumption that $\boldsymbol{A}^{-1} \approx (\boldsymbol{A} + z^{-1}_{\text{aug,par},1}\boldsymbol{\xi}_1\boldsymbol{\xi}_1^{\text{t}})^{-1}$. As mentioned in Section 3.4, this is due to augmentation being a small refinement and thus should have a relatively small effect on $\boldsymbol{A}^{-1}$.

In the case where this error is not negligible, refinement iterations can be used to further optimize the augmentations. The general process used is as follows:

1. Using the algorithm proposed in Section 3.4, determine an initial frequency-dependent driving-point impedance for each augmentation.

2. For each augmentation, in sequence, perform the following:

   (a) Insert every augmentation except the current one into the original S-ECM.

   (b) Using the parallel augmentation algorithm presented in Section 3.2 or the series augmentation algorithm in Section 3.3, as appropriate, determine a new driving-point impedance for the augmentation under consideration.

3. Iterate over Step 2 until the error is reduced to an acceptable level.

It is noted that the multiple augmentation algorithm in Section 3.4 produces a rational function for each augmentation's driving point impedance. On the other hand, the single augmentation algorithms of Sections 3.2 to 3.3 produce a set of tabulated data. Therefore, prior to synthesizing the augmentation, this data must

be fit to a rational function, as will be discussed in the next section. This fitting can occur during each iteration after finding the new data for the augmentation or it can be done once at the end of the procedure. It is left for future study to determine which of these options is optimal for most cases.

In addition, for synthesis to be possible, the rational function must represent a passive network. As with the rational function fit, passivity enforcement can be applied at either of these points as well. Once again, it is left to future research to determine when to best perform this.

5.3 Choice of Fitting Function

In Chapter 3, a method is presented to determine an appropriate driving-point impedance for each of a set of augmenting networks to improve the performance of a device model. In the case of fitting multiple augmentations at once, in Section 3.4, the method of producing the final rational functions is specified by the algorithm. In that case, the rational functions are found by optimizing the numerator and denominator coefficients of the rational function in a least-squares sense.

On the other hand, in the case where a single augmenting network is being found, the resulting driving-point impedance is a set of tabulated data. This leaves the method used to produce a rational function for the driving-point impedance as an open question.

One option is to use the same method as is used for the multiple augmentations, coefficient fitting. For this method, a new function $z_{\text{aug,fit}}(s)$ is defined with the form

$$z_{\text{aug,fit}}(s) = \frac{a_0 + a_1 s + \cdots + a_p s^p}{b_0 + b_1 s + \cdots + b_{q-1} s^{q-1} + s^q} \tag{5.7}$$

such that it minimizes the error function

$$\epsilon = \sum_{i=1}^{n} \| z_{\text{aug,fit}}(\jmath\omega_i) - z_{\text{aug}}[\omega_i] \| \tag{5.8}$$

where z_{aug} represents the tabulated driving-point impedance data, sampled over n frequency points given by $\{\omega_1, \cdots, \omega_n\}$.

This can be accomplished if the coefficients are found through the optimal solution of the following over-determined system.

$$\begin{bmatrix}
1 & 0 & -\omega_1^2 & 0 & \cdots & \text{Re}\{(\jmath\omega_1)^p\} & -\text{Re}\{z_{\text{aug}}[\omega_1]\} \\
0 & \omega_1 & 0 & -\omega_1^3 & \cdots & \text{Im}\{(\jmath\omega_1)^p\} & -\text{Im}\{z_{\text{aug}}[\omega_1]\} \\
\vdots & \vdots & \vdots & \vdots & \ddots & \vdots & \vdots \\
1 & 0 & -\omega_n^2 & 0 & \cdots & \text{Re}\{(\jmath\omega_n)^p\} & -\text{Re}\{z_{\text{aug}}[\omega_n]\} \\
0 & \omega_n & 0 & -\omega_n^3 & \cdots & \text{Im}\{(\jmath\omega_n)^p\} & -\text{Im}\{z_{\text{aug}}[\omega_n]\}
\end{bmatrix}$$

$$\begin{bmatrix}
-\text{Re}\{z_{\text{aug}}[\omega_1]\jmath\omega_1\} & \cdots & -\text{Re}\{z_{\text{aug}}[\omega_1](\jmath\omega_1)^{q-1}\} \\
-\text{Im}\{z_{\text{aug}}[\omega_1]\jmath\omega_1\} & \cdots & -\text{Im}\{z_{\text{aug}}[\omega_1](\jmath\omega_1)^{q-1}\} \\
\vdots & \ddots & \vdots \\
-\text{Re}\{z_{\text{aug}}[\omega_n]\jmath\omega_n\} & \cdots & -\text{Re}\{z_{\text{aug}}[\omega_n](\jmath\omega_n)^{q-1}\} \\
-\text{Im}\{z_{\text{aug}}[\omega_n]\jmath\omega_n\} & \cdots & -\text{Im}\{z_{\text{aug}}[\omega_n](\jmath\omega_n)^{q-1}\}
\end{bmatrix}
\begin{bmatrix} a_0 \\ \vdots \\ a_p \\ b_0 \\ \vdots \\ b_{q-1} \end{bmatrix}
=
\begin{bmatrix}
\text{Re}\{z_{\text{aug}}[\omega_1](\jmath\omega_1)^q\} \\
\text{Im}\{z_{\text{aug}}[\omega_1](\jmath\omega_1)^q\} \\
\vdots \\
\text{Re}\{z_{\text{aug}}[\omega_n](\jmath\omega_n)^q\} \\
\text{Im}\{z_{\text{aug}}[\omega_n](\jmath\omega_n)^q\}
\end{bmatrix} \tag{5.9}$$

There are many other fitting algorithms available that will also produce a rational function representation for the data found for z_{aug}. One popular alternative is vector fitting [11]. Instead of fitting the coefficients of the rational function directly, this method identifies the dominant poles in a response and then finds the corresponding residues. In the transmission line examples in Chapter 4, it was found that using vector fit produced superior results.

5.4 Frequency Scaling

For any of the possible rational function fitting methods, it is usually of benefit to perform frequency scaling. Frequency scaling is the uniform scaling of the actual frequency values to improve the numerical condition of the fitting matrices. The problem can be seen by examining the matrix in (5.9). The system contains elements where the frequencies are being raised by powers related to the number of numerator or denominator coefficients. As more coefficients are added to fit a more complex function, the highest power seen in the matrix will increase.

To illustrate the effect of this, the following matrix is considered.

$$\boldsymbol{A} = \begin{bmatrix} 1 & 0 & -\omega_1^2 & 0 & \cdots & \mathrm{Re}\{(\jmath\omega_1)^p\} \\ 0 & \omega_1 & 0 & -\omega_1^3 & \cdots & \mathrm{Im}\{(\jmath\omega_1)^p\} \\ \vdots & \vdots & \vdots & \vdots & \ddots & \vdots \\ 1 & 0 & -\omega_n^2 & 0 & \cdots & \mathrm{Re}\{(\jmath\omega_n)^p\} \\ 0 & \omega_n & 0 & -\omega_n^3 & \cdots & \mathrm{Im}\{(\jmath\omega_n)^p\} \end{bmatrix} \tag{5.10}$$

This is recognizable as being a section from the system of (5.9). Let p and n be 5, and $\boldsymbol{\omega}$ be a set of equally spaced frequency points between 1 Mrad/s and 10 Grad/s, or

$$\boldsymbol{\omega} = \{\omega_1, \omega_2, \omega_3, \omega_4, \omega_5\} = \{1 \times 10^6, 2.5008 \times 10^9, 5.0005 \times 10^9, 7.5002 \times 10^9, 1 \times 10^{10}\} \tag{5.11}$$

Next, scaling is introduced to this system. Let $\alpha \in \Re$ be the scaling factor. Define $\hat{\omega}$ as the scaled version of $\boldsymbol{\omega}$ and $\hat{\boldsymbol{A}}$ as the scaled version of $\boldsymbol{A}$. These are given by

$$\hat{\omega} = \left\{\frac{\omega_1}{\alpha}, \frac{\omega_2}{\alpha}, \frac{\omega_3}{\alpha}, \frac{\omega_4}{\alpha}, \frac{\omega_5}{\alpha}\right\} \tag{5.12}$$

$$\hat{\boldsymbol{A}} = \begin{bmatrix} 1 & 0 & -\left(\frac{\omega_1}{\alpha}\right)^2 & 0 & \cdots & \mathrm{Re}\left\{\left(\frac{\jmath\omega_1}{\alpha}\right)^p\right\} \\ 0 & \frac{\omega_1}{\alpha} & 0 & -\left(\frac{\omega_1}{\alpha}\right)^3 & \cdots & \mathrm{Im}\left\{\left(\frac{\jmath\omega_1}{\alpha}\right)^p\right\} \\ \vdots & \vdots & \vdots & \vdots & \ddots & \vdots \\ 1 & 0 & -\left(\frac{\omega_n}{\alpha}\right)^2 & 0 & \cdots & \mathrm{Re}\left\{\left(\frac{\jmath\omega_n}{\alpha}\right)^p\right\} \\ 0 & \frac{\omega_n}{\alpha} & 0 & -\left(\frac{\omega_n}{\alpha}\right)^3 & \cdots & \mathrm{Im}\left\{\left(\frac{\jmath\omega_n}{\alpha}\right)^p\right\} \end{bmatrix} \tag{5.13}$$

Table 5.1: Effect of Frequency Scaling on Reciprocal Condition

α	reciprocal condition of $\hat{\boldsymbol{A}}^{\mathrm{t}}\hat{\boldsymbol{A}}$
1	7.0608×10^{-82}
10^9	6.761×10^{-10}
10^{10}	6.4892×10^{-4}
10^{11}	5.184×10^{-11}

The reciprocal of the condition of a matrix in the 1-norm is a measure of how well-conditioned a matrix is [27]. A well-conditioned matrix has a reciprocal condition close to 1, while in poorly conditioned matrices it approaches ∞^{-1}. When a matrix is poorly conditioned, it is a nearly singular matrix, which increases the error resulting from numerical processes.

Table 5.1 shows the effect on the reciprocal condition of $\hat{\boldsymbol{A}}^{\mathrm{t}}\hat{\boldsymbol{A}}$ due to scaling $\boldsymbol{\omega}$ by different amounts. It is seen that the choice of α is very important. In this case, choosing α to be the largest value in $\boldsymbol{\omega}$ was optimal.

To see the effect of this on a more practical application, consider the use of scaling in the system of (5.9). Clearly, if the frequencies are scaled, this will have an effect on the coefficients that are found. After scaling, the rational function in (5.7) will become the following

$$z_{\mathrm{aug,fit}}(\jmath\omega) = \frac{\hat{a}_0 + \hat{a}_1\left(\frac{\jmath\omega}{\alpha}\right) + \cdots + \hat{a}_p\left(\frac{\jmath\omega}{\alpha}\right)^p}{\hat{b}_0 + \hat{b}_1\left(\frac{\jmath\omega}{\alpha}\right) + \cdots + \hat{b}_{q-1}\left(\frac{\jmath\omega}{\alpha}\right)^{q-1} + \left(\frac{\jmath\omega}{\alpha}\right)^q} \tag{5.14}$$

To convert this back to the form of (5.7), the right-hand side is multiplied by $\frac{\alpha^q}{\alpha^q}$, which results in

$$z_{\text{aug,fit}}(\jmath\omega) = \frac{\hat{a}_0\alpha^q + \hat{a}_1\alpha^{q-1}\jmath\omega + \cdots + \hat{a}_p\alpha^{q-p}(\jmath\omega)^p}{\hat{b}_0\alpha^q + \hat{b}_1\alpha^{q-1}\jmath\omega + \cdots + \hat{b}_{q-1}\alpha(\jmath\omega)^{q-1} + (\jmath\omega)^q} \tag{5.15}$$

Therefore, when frequency scaling is used, the actual coefficients of the rational function are given by

$$\begin{bmatrix} a_0 \\ a_1 \\ \vdots \\ a_{p-1} \\ a_p \\ b_0 \\ b_1 \\ \vdots \\ b_{q-2} \\ b_{q-1} \end{bmatrix} = \begin{bmatrix} \hat{a}_0\alpha^q \\ \hat{a}_1\alpha^{q-1} \\ \vdots \\ \hat{a}_{p-1}\alpha^{q-p+1} \\ \hat{a}_p\alpha^{q-p} \\ \hat{b}_0\alpha^q \\ \hat{b}_1\alpha^{q-1} \\ \vdots \\ \hat{b}_{q-2}\alpha^2 \\ \hat{b}_{q-1}\alpha \end{bmatrix} \tag{5.16}$$

5.5 Frequency Weighting

When fitting the coefficients of a rational function to a driving-point impedance, the goal is to reduce the error over the entire frequency range of interest. In most cases, it is desired to improve this error by the same relative amount for each frequency

point. However, with the standard formulation, this is often not the case.

Examining the rows of (5.9), it is observed that each row corresponds to a single frequency point. In addition, each element containing z_{aug} is also being multiplied by that frequency raised to a power. This implies that rows corresponding to higher frequencies will have larger values, which will weight their errors higher while being solved in a least squares sense.

To overcome this difficulty, the individual rows can be weighted by an arbitrary constant. If both the left-hand side and the right-hand side of an equation are multiplied by the same constant, it has no effect. Therefore, rows for lower frequencies can be multiplied by a larger constant than rows for higher frequencies. Doing this will help balance the error reduction effort and improve the lower frequencies by a similar amount as the higher ones.

5.6 Summary

In this chapter, various implementation issues concerning the algorithm developed in Chapters 3 and 4 were discussed. First, a means to overcome the error introduced during the multiple augmentation procedure of Section 3.4 was given. The remaining sections covered the rational function fit of tabulated data and various methods to help improve the quality of the fit.

Chapter 6

Conclusions and Future Work

6.1 Summary

In this thesis, an efficient and automated algorithm was presented which identifies augmenting equivalent circuits to improve the accuracy of simple equivalent-circuit models (S-ECMs) over a frequency range of interest. This algorithm is generic in the sense that it can be applied to any multi-port equivalent-circuit model for a device whose performance can be described by y-parameters. Therefore, it has a wide range of applications. In the initial algorithm development (in Chapter 3), it was applied to a small-signal model for a FET transistor and also to a model for a spiral inductor. In Chapter 4, the algorithm was applied to frequency-dependent transmission lines. The algorithm was also extended to handle mutual inductances,

so that coupled frequency-dependent transmission lines could be created. Finally, in Chapter 5, various important implementation issues were discussed. The most important advantages to this approach are as follows:

1. This algorithm uses and develops equivalent-circuit models for devices. When an appropriate S-ECM is chosen, this technique allows the physical intuitiveness of the model to be maintained while providing a good match with the measurements of a physical device. This can be of great importance to designers, who prefer these types of models to purely mathematical ones.

2. All of the optimization problems used by the algorithm are formulated as linear optimization problems. Nonlinear optimization formulations can have issues with convergence, local minima, and CPU time cost.

3. The models that are created are easy to use in both frequency- and time-domain simulators. This is a particular advantage to the frequency-dependent transmission line models, as signal integrity simulations are generally performed in the time domain.

4. The algorithm is generic, so it should be applicable to any sort of device with an associated simple equivalent-circuit model.

5. The algorithm produces augmenting networks in the form of single-port networks whose driving-point impedances are described by rational functions.

This greatly simplifies the existing passivity enforcement mechanisms [12] allowing for a more efficient implementation.

6.2 Future Work

Through the work in this thesis, many possibilities for future research have become apparent. These are summarized below.

1. **Application to large-scale sensitivity:** This work is closely related to the large-scale sensitivity. One area of future research would be to investigate if any of the techniques developed in this thesis could be applied to improve or gain more insight into the large-scale sensitivity analysis process.

2. **Integration of element perturbation:** It is conceivable that in many cases a full augmentation may not be needed to correct the error in some locations. It would be interesting to investigate the impact of perturbing the existing model elements in conjunction with large-scale augmentations. This would be similar to the approach of improving black-box augmentation discussed in [9].

3. **Application to modelling emerging device effects:** There is a lot of research opportunities in the application of this algorithm to many types

of models, from device models to spiral inductors. Instead of the traditional methods of improving equivalent-circuit models, the proposed algorithm could be applied to model emerging effects in high-frequency operation.

4. **Nonlinear device modelling:** Another area to be studied is the application of this method to nonlinear models. It might be possible to include nonlinear elements in the augmentations and also to augment models with existing nonlinear elements.

References

[1] S. K. Mandal, A. De, A. Patra, and S. Sural, "A wide-band lumped element compact cad model of si-based planar spiral inductor for rfic design," in *Proc. 19th International Conference on VLSI Design*, Hyderabad, India, Jan. 2006.

[2] C. J. Chao, S. C. Wong, *et al.*, "Characterization and modeling of on-chip inductor substrate coupling effect," in *Proc. IEEE MTT-S International Microwave Symposium (IMS2002)*, Seattle, WA, June 2002, pp. 157–160.

[3] J. Wang and K. Wu, "A derived physically expressive circuit model for multi-layer rf embedded passives," *IEEE Transactions on Microwave Theory and Techniques*, vol. 54, no. 5, pp. 1961–1968, May 2006.

[4] A. Scuderi, T. Biondi, *et al.*, "A scalable model for silicon spiral inductors," in *Proc. IEEE MTT-S International Microwave Symposium (IMS2003)*, Philadelphia, PA, June 2003, pp. 2117–2120.

[5] D. Melendy, P. Francis, *et al.*, "Wide-band compact modeling of spiral inductors in RFICs," in *Proc. IEEE MTT-S International Microwave Symposium (IMS2002)*, Seattle, WA, June 2002, pp. 717–720.

[6] A. Watson, D. Melendy, P. Francis, K. Hwang, and A. Weisshaar, "A comprehensive compact modeling methodology for spiral inductors in silicon-based RFICs," *IEEE Transactions on Microwave Theory and Techniques*, vol. 52, no. 3, pp. 849–857, Mar. 2004.

[7] G. D. Vendelin, A. M. Pavio, and U. L. Rohde, *Microwave Circuit Design Using Linear and Nonlinear Techniques.* New York: John Wiley & Sons, 1990, p. 468.

[8] J. Kolstad, C. Blevins, J. Dunn, and A. Weisshaar, "A new modeling methodology for passive components based on black-box augmentation combined with equivalent circuit perturbation," in *Proc. IEEE Topical Meeting on Electrical Performance of Electronic Packaging (13th EPEP)*, Portland, OR, Oct. 2004, pp. 259–262.

[9] J. Kolstad, C. Blevins, J. M. Dunn, and A. Weisshaar, "A new circuit augmentation method for modeling of interconnects and passive components," *IEEE Transactions on Advanced Packaging*, vol. 29, no. 1, pp. 67–77, Feb. 2006.

[10] R. Achar and M. S. Nakhla, "Simulation of high-speed interconnects," *Proc. IEEE*, pp. 693–728, May 2001.

[11] D. Saraswat, R. Achar, and M. S. Nakhla, "A fast algorithm and practical considerations for passive macromodeling of measured/simulated data," *IEEE Transactions on Advanced Packaging*, vol. 27, no. 1, pp. 57–70, Feb. 2004.

[12] B. Gustavsen and A. Semlyen, "Enforcing passivity for admittance matrices approximated by rational functions," *IEEE Transactions on Power Systems*, vol. 16, pp. 97–104, Feb. 2001.

[13] D. Saraswat, R. Achar, and M. Nakhla, "Global passivity enforcement algorithm for macromodels of interconnect subnetworks characterized by tabulated data," *IEEE Transactions on Very Large Scale Integration (VLSI) Systems*, vol. 13, no. 7, pp. 819–832, July 2005.

[14] L. Weinberg, *Network Analysis and Synthesis.* New York: McGraw-Hill, 1962.

[15] O. Brune, "Synthesis of a finite two-terminal network whose driving-point impedance is a prescribed function of frequency," *Journal of Mathematical Physics*, vol. 10, pp. 191–236, 1931.

[16] D. Paul, M. S. Nakhla, R. Achar, and A. Weisshaar, "Broadband macromodelling of high-speed passive modules," in *Proc. 10th IEEE Workshop on Signal Propagation on Interconnects (SPI2006)*, Berlin, Germany, May 2006.

[17] ——, "An automated algorithm for broadband modeling of high-frequency microwave devices," in *Proc. IEEE MTT-S International Microwave Symposium (IMS2006)*, San Francisco, CA, June 2006, pp. 1767–1770.

[18] ——, "Broadband modeling of high-frequency microwave devices," in *IEEE Transactions on Microwave Theory and Techniques*, under preparation, to be submitted.

[19] ——, "A passive algorithm for modeling frequency-dependent parameters of coupled interconnects," in *Proc. IEEE Topical Meeting on Electrical Performance of Electronic Packaging (15th EPEP)*, Scottsdale, AZ, Oct. 2006, to be published.

[20] J. Vlach and K. Singhal, *Computer Methods for Circuit Analysis and Design.* New York: Van Nostrand, 1983.

[21] R. A. Rohrer, "Circuit partitioning simplified," *IEEE Transactions on Circuits and Systems*, vol. 35, no. 1, pp. 2–5, Jan. 1988.

[22] J. Sherman and W. J. Morrison, "Adjustment of an inverse matrix corresponding to changes in the elements of a given column or a given row of the original matrix," *The Annals of Mathematical Statistics*, vol. 20, 1949.

[23] A. S. Householder, "A survey of some closed methods for inverting matrices," *Journal of the Society for Industrial and Applied Mathematics*, vol. 5, no. 3, pp. 155–169, Sept. 1957.

[24] A. Watson, "Analysis and modeling of single-ended and differential spiral inductors in silicon-based RFICs," Master's thesis, Oregon State University, Portland, OR, 2003.

[25] C. R. Paul, *Analysis of Multiconductor Transmission Lines.* New York: Wiley, 1994.

[26] A. E. Ruehli, A. C. Cangellaris, and H.-M. Huang, "Three test problems for the comparison of lossy transmission line algorithms," in *Proc. IEEE Topical Meeting on Electrical Performance of Electronic Packaging (11th EPEP)*, Monterrey, CA, Oct. 2002, pp. 347–350.

[27] E. Anderson, Z. Bai, C. Bischof, *et al.*, *LAPACK User's Guide.* Philadelphia: SIAM, 1999.